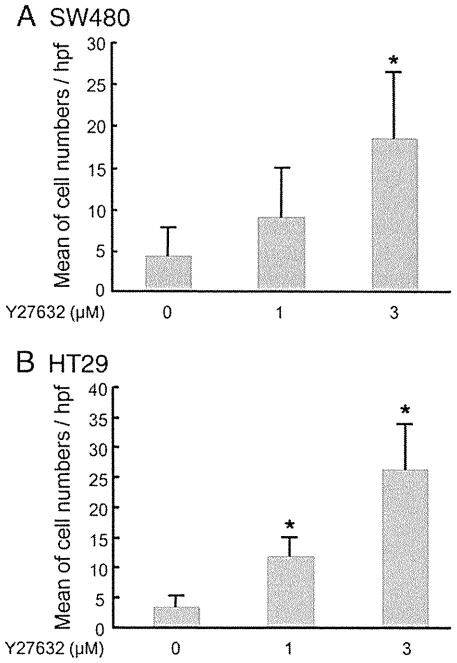

Fig. 1. The effects of Y27632 on the migration of SW480 and HT29 colon cancer cells. The SW480 (A) and HT29 (B) cells (5×10^4 per well) were seeded in the upper Boyden chamber in DMEM containing 10% fetal calf serum, and after 24 h incubation, various concentrations of Y27632 were added to the bottom chamber and cells were incubated for an additional 48 h at 37 °C. Next, the remaining cells on the upper surface of the membrane were mechanically removed, and the cells that had migrated to the lower surface of the membrane were fixed and stained with hematoxylin. The average number of migrated cells from 5 randomly chosen fields on the lower surface of the membrane was counted. Each value represents the mean ± S.E.M. of triplicate independent determinations. * indicates a significant increase ($P<0.05$) compared with the control (lane 1, respectively).

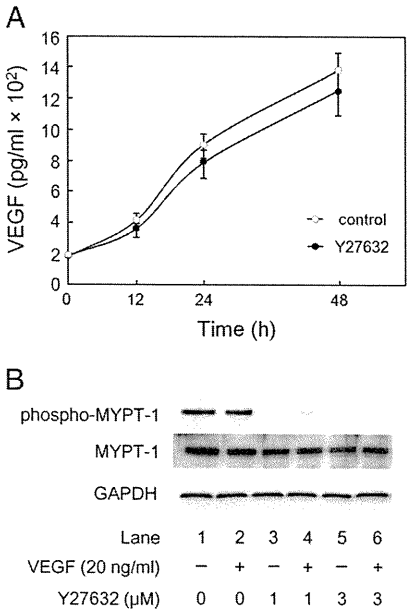

Fig. 2. (A) The effect of Y27632 on VEGF release in SW480 colon cancer cells. After incubation in the medium containing 10% fetal calf serum, the cells were cultured in fresh medium without serum and incubated for the indicated periods. The respective media were then collected, and the VEGF concentration was measured by ELISA (see Materials and Methods). Open circle (○): untreated control cells. Closed circle (●): 3 μM of Y27632-treated cells. Each value represents the mean ± S.E.M. of triplicate independent determinations. (B) The effects of VEGF and Y27632 on the phosphorylation of MYPT-1 in SW480 colon cancer cells. SW480 cells were pretreated with various concentrations of Y27632 for 60 min, followed by exposure to 20 ng/mL of VEGF or vehicle for 20 min. The extracts of cells were then subjected to sodium dodecyl sulfate-polyacrylamide gel electrophoresis (SDS-PAGE) and were then subjected to the Western blot analysis with antibodies against phospho-specific MYPT-1, MYPT-1 and GAPDH.

migration and vascular permeability, all of which can lead to metastasis (Pourgholami and Morris, 2008). Therefore, we next measured the VEGF concentration in the medium of SW480 cells to determine whether these cells are able to produce VEGF. After incubation of the cells in the medium containing 10% fetal calf serum, they were cultured in fresh medium without serum for the indicated periods. As a result, the VEGF concentration was gradually increased (Fig. 2A, open circle), thus suggesting that SW480 cells can produce VEGF.

Since we found that Y27632 caused the migration of colon cancer cells (as described above; Fig. 1), we next investigated the effect of Y27632 on VEGF release from SW480 cells. However, Y27632 did not affect its release (Fig. 2A, closed circle). This suggests that the increase in migration by the cells incubated with Y27632 is not due to an increase in VEGF release from the SW480 cells.

3.3. Effect of exogenous VEGF on Rho-kinase activity in SW480 colon cancer cells

We next examined the effect of exogenous VEGF on the levels of phosphorylated MYPT-1, which is a component of myosin phosphatase and well known as a downstream substrate of Rho-kinase (Riento and Ridley, 2003). We observed that MYPT-1 was phosphorylated even in untreated SW480 cells (Fig. 2B, lane 1), which is consistent with our previous study (Nakashima et al., 2010). However, when the cells were exposed to exogenous VEGF, the phosphorylated levels of MYPT-1 was not affected (Fig. 2B, lane 2 compared to lane 1). We also examined the effect of various concentrations of VEGF for different periods of time (up to 180 min) on the phosphorylation of MYPT-1, but did not observe any increase in the phosphorylation level (data not shown). However, we verified that Y27632 clearly suppressed the phosphorylation of MYPT-1 at a concentration of 1 μM or greater (Fig. 2B, lanes 3 to 6), while Y27632 did not affect the total protein levels of MYPT-1 (Fig. 2B, lower panel). Based on our findings, it is most likely that Rho-kinase is generally in an activated state in unstimulated SW480 cells, and exogenous VEGF therefore has little effect on the activation of Rho-kinase in these cells.

3.4. Effect of Rho-kinase inhibitor on the localization of focal adhesion components in SW480 colon cancer cells

We next performed an immunofluorescence microscopy study to observe the abundance and localization of several cytoskeletal proteins, such as vinculin, because cell migration involves changes in the cytoskeleton and cell adhesion (Ridley et al., 2003). In untreated SW480 cells, vinculin, which is a characteristic feature of focal adhesion formation (Brew et al., 2009), was strongly stained on focal adhesions around the cell periphery (Fig. 3, panel 1), where the stress fiber terminates (Brew et al., 2009). When SW480 cells were pretreated with Y27632, there was a marked loss in the size and number of focal adhesions (as indicated by vinculin staining) around the cell periphery (Fig. 3, panel 2 compared to panel 1). Moreover, the expression and localization of phosphorylated caveolin-1, another component of the focal adhesion complex (Joshi et al., 2008), were similar to vinculin (Fig. 3, panel 3), and incubation with Y27632 also caused the loss of the localization of phosphorylated caveolin-1 (Fig. 3, panel 4).

Several non-receptor protein kinases, including members of the Src family and FAK, are involved in the organization of molecular adhesion complexes (Burridge and Chrzanowska-Wodnicka, 1996;

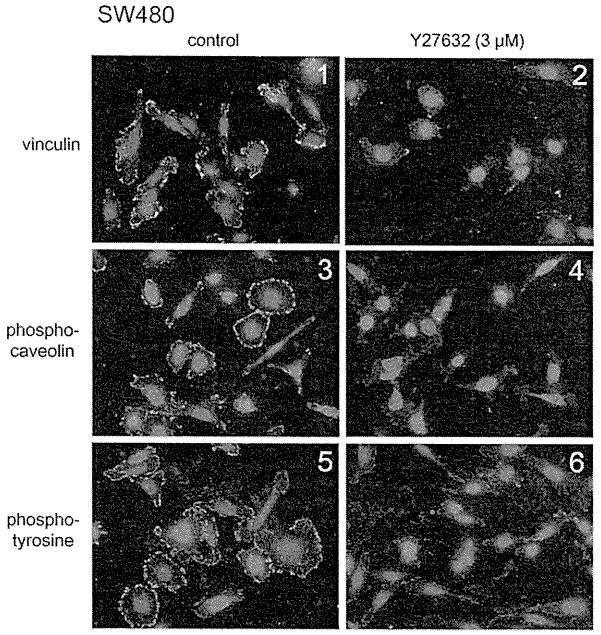

Fig. 3. The effect of Y27632 on the formation of focal adhesion complexes in SW480 colon cancer cells. SW480 cells grown on coverslip-bottom dishes were incubated with (panels 2, 4 and 6) or without Y27632 (panels 1, 3 and 5) for 60 min at 37 °C. After fixation, the cells were exposed to anti-vinculin antibodies (panels 1 and 2), anti-phospho-caveolin-1 antibodies (panels 3 and 4) and anti-phosphotyrosine antibodies (panels 5 and 6), followed by exposure to Alexa Fluor 488® conjugated secondary antibodies and DAPI for 60 min. The cells were then examined by fluorescence microscopy.

Humphries et al., 2007) and they regulate the signaling events that occur at focal adhesions (Wozniak et al., 2004). To examine the effect of Y27632 on the localization of tyrosine-phosphorylated proteins at focal adhesions, we used antibodies against pan-phosphotyrosine. In untreated SW480 cells, anti-phosphotyrosine staining was concentrated mostly at the cell edges, similar to that observed for vinculin or phosphorylated caveolin-1. Y27632 also caused the loss of localization of these tyrosine-phosphorylated proteins (Fig. 3, panels 5 and 6). These results suggest that Y27632 causes a dramatic change in the localization of focal adhesion components such as vinculin, phosphorylated caveolin-1 and tyrosine-phosphorylated proteins, thereby supporting our findings that Y27632 induced the migration of colon cancer cells as shown in Fig. 1.

3.5. Effect of Rho-kinase inhibitor on the Akt pathway in SW480 colon cancer cells

We next investigated the effect of Y27632 on the Akt pathway in SW480 cells. Y27632 markedly induced the phosphorylation of Akt in a time-dependent manner (Fig. 4A). The effect of Y27632 on the phosphorylation of Akt was observed within 1 h and reached its maximum at 3 h, and decreased thereafter. We also observed a similar effect in the cells treated with another Rho-kinase inhibitor, fasudil (Shimokawa and Rashid, 2007) (data not shown).

GSK-3β is a critical downstream element of the PI3K/Akt cell survival pathway, and its activity can be inhibited by Akt-mediated phosphorylation (Cross et al., 1995). Therefore, we next examined the effect of Y27632 on the level of phosphorylated GSK-3β. Y27632 caused the phosphorylation of GSK-3β within 30 min, which was sustained for 24 h, and decreased thereafter (Fig. 4A). We further confirmed that Y27632-induced phosphorylation of Akt was significantly suppressed when the cells were treated with Akt inhibitor.

3.6. The involvement of the Akt pathway in the Y27632-induced alteration of focal adhesion formation in SW480 and HT29 colon cancer cells

As described earlier, we showed strong staining with vinculin in the focal adhesions around the cell periphery in untreated SW480 cells (Fig. 3, panel 1), and that Y27632 caused a decrease in the size and number of focal adhesions (Fig. 3, panel 2). Therefore, we next investigated the involvement of Akt in focal adhesion formation. As shown in Fig. 4C, the inhibition of Akt restored the size and number of focal adhesions that stained for vinculin in the SW480 cells incubated

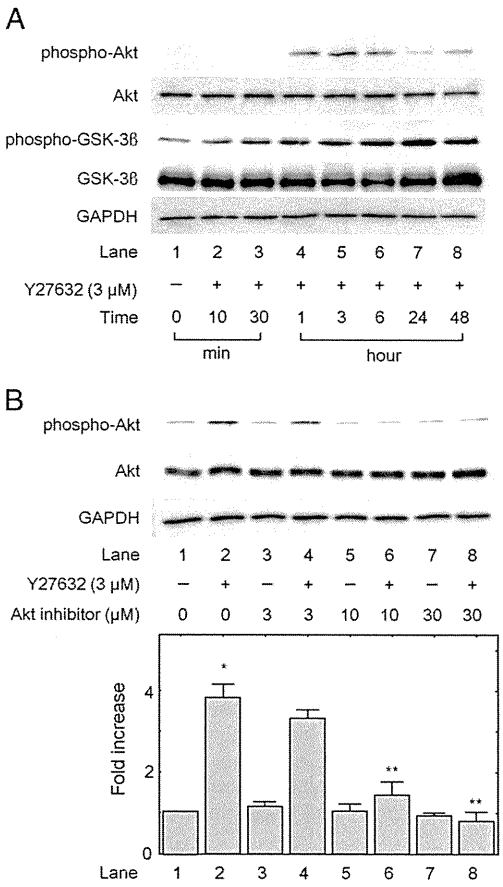

Fig. 4. The involvement of Akt in SW480 cell migration. (A) The effect of Y27632 on the phosphorylation of Akt and GSK-3β in SW480 colon cancer cells. Cells were pretreated with 3 μM of Y27632 for the indicated periods, and the extracts of cells were then subjected to sodium dodecyl sulfate-polyacrylamide gel electrophoresis (SDS-PAGE) and a Western blot analysis with antibodies against phospho-specific Akt, Akt, phospho-specific GSK-3β, GSK-3β and GAPDH as a loading control. (B) The effect of the Akt inhibitor on Y27632-induced phosphorylation of Akt in SW480 colon cancer cells. The cells were pretreated with the indicated concentrations of Akt inhibitor for 60 min, and then were exposed to 3 μM of Y27632 for 60 min. The extracts of cells were then subjected to SDS-PAGE and a Western blot analysis with antibodies against phospho-specific Akt, Akt and GAPDH as a loading control. The lower bar graph shows the quantification data for the relative levels of phospho-Akt, after normalization with respect to total Akt, as determined by densitometry. Each value represents the mean ± S.E.M. of triplicate independent determinations. * indicates a significant increase ($P<0.05$, compared with lane 1) and ** indicates a significant decrease ($P<0.05$, compared with lane 2). (C and D) The effect of the Akt inhibitor on Y27632-induced alteration of the localization of focal adhesion molecule, vinculin, in SW480 (C) and HT29 (D) colon cancer cells. The cells grown on coverslip-bottom dishes were pretreated with or without the Akt inhibitor (10 μM) for 60 min and then incubated with or without Y27632 (3 μM) for 60 min at 37 °C. After fixation, the cells were then exposed to anti-vinculin antibodies, followed by exposure to Alexa Fluor 488® conjugated secondary antibodies and DAPI for 60 min. The cells were then examined by fluorescence microscopy.

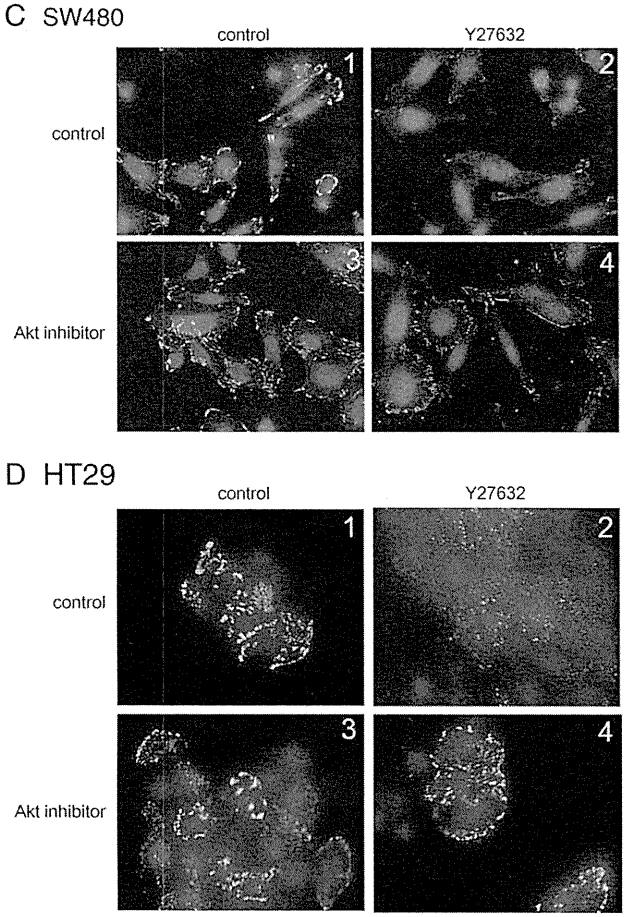

Fig. 4 (*continued*).

with Y27632 (Fig. 4C, panel 4 compared to panel 2). Similarly, we observed that the Akt inhibitor significantly restored the loss of focal adhesion induced by Y27632 in HT29 cells (Fig. 4D). These results suggest that the alteration of focal adhesion formation induced by Y27632 is mediated through the Akt pathway in colon cancer cells.

4. Discussion

Because metastasis is common among many types of cancer, and is related to the prognosis of most cancers, researchers have expanded their interests into the anti-invasive and anti-angiogenic compounds that do not directly to kill tumor cells, such as matrix metalloproteinase (MMP) inhibitors or anti-vascular endothelial growth factor (VEGF) antibodies (Egeblad and Werb, 2002; Kerbel and Folkman, 2002). In the present study, we investigated the role of Rho-kinase in the migration of SW480 colon cancer cells. We have recently reported that Rho-kinase negatively regulates EGF-induced cell proliferation at a point upstream of Akt/GSK-3β in colon cancer cells (Nakashima et al., 2010). EGF-induced phosphorylation of Akt and GSK-3β, and the subsequent increase in the phosphorylation of the retinoblastoma tumor suppressor protein, as well as an increase in the cyclin D1 protein expression level, were dose-dependently enhanced when the cells were pretreated with Y27632 (Nakashima et al., 2010). In this study, we found that the inhibition of Rho-kinase caused an increase in cell migration (Fig. 1), thus suggesting that Rho-kinase is involved not only in cell cycle progression, but also in the migration of colon cancer cells.

VEGF has been previously shown to induce the migration of colon cancer cells (Diaz-Rubio, 2006). Although SW480 cells can produce VEGF (Fig. 2A), the cell migration induced by Y27632 was not due to an increase in VEGF release from SW480 cells (Fig. 2A), thus indicating that Rho-kinase is not involved in the process of VEGF release. Moreover, it has recently been suggested that VEGF has both a positive and a negative regulatory effect on tumor growth (Vecchiarelli-Federico et al., 2010). Although we showed that Rho-kinase was strongly activated at baseline in our colon cancer cell line, we speculate that VEGF released in an autocrine manner from SW480 cells might regulate the migration of these cells via suppression of Rho-kinase.

We next performed an immunofluorescence microscopy study to observe the effect of Y27632 on the localization of focal adhesion molecules, such as vinculin, caveolin-1 and tyrosine-phosphorylated proteins (Fig. 3). We thus showed that Y27632 caused a marked loss in the size and number of focal adhesions around the cell periphery, as revealed by vinculin staining (Fig. 3, panel 2 compared to panel 1). Staining with antibodies against phosphorylated caveolin-1 and phosphotyrosine showed similar results (Fig. 3, panels 3–6). These findings strongly suggest that the inhibition of Rho-kinase causes the marked decrease in the formation of the focal adhesion complex, indicating that Rho-kinase negatively regulates colon cancer cell migration.

We further examined the mechanism underlying Y27632-induced cell migration in colon cancer cells. We first found that Y27632 induced the activation of Akt and GSK-3β (Fig. 4). We also observed that Y27632 failed to affect the phosphorylation of p44/p42 mitogen-activated protein kinase (MAPK), p38 MAPK and stress-activated protein kinase/c-*Jun* N-terminal kinase (data not shown). Y27632-induced activation of Akt was suppressed by pretreatment with an Akt-specific inhibitor (Fig. 4B). Interestingly, we demonstrated the Y27632-induced loss of the localization of vinculin to be restored when the cells were pretreated with the Akt inhibitor (Fig. 4C), thus suggesting that Rho-kinase negatively regulates the formation of focal adhesion via the Akt pathway in colon cancer cells. Moreover, we observed similar results in HT29 cells (Fig. 4D), thus suggesting that these results are not confined to a specific cell line. A schematic representation of the involvement of Rho-kinase in the migration of colon cancer cells is shown in Fig. 5.

The Rho/Rho-kinase pathway takes part in cancer progression by regulating actin cytoskeleton reorganization. Since a specific Rho-kinase inhibitor was found to suppress tumor growth and metastasis (Itoh et al., 1999), it has been reported that the Rho/Rho-kinase pathway may become a molecular target for the prevention of cancer invasion and metastasis. In contrast, a recent study showed the

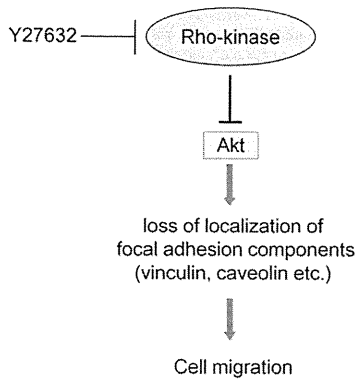

Fig. 5. A schematic representation of the involvement of Rho-kinase in the migration of colon cancer cells. In unstimulated colon cancer cells, Rho-kinase is generally activated at baseline, and suppresses the activation of Akt, which induces the loss of localization of focal adhesion components (vinculin, caveolin, etc.) and leads to cell migration. Therefore, the inhibition of Rho-kinase by Y27632 causes activation of Akt, indicating that Rho-kinase negatively regulates the migration of colon cancer cells.

activation of Rho-kinase to lead to an inhibition of motility in human breast cancer cells (Brew et al., 2009). In this report, indole-3-carbinol (I3C), a phytochemical derived from cruciferous vegetables, was shown to decrease metastatic spread of tumors in experimental animals, and I3C induced stress fibers and peripheral focal adhesions in a Rho-kinase-dependent manner (Brew et al., 2009). In addition, Y27632, a specific Rho-kinase inhibitor, reportedly interferes with Ras-mediated transformation, and constitutively active form of mutant Rho-kinase collaborate with activated Raf in transformation assays in NIH3T3 fibroblastic cells (Sahai et al., 1999). On the other hand, the inactivation of the Rho/Rho-kinase pathway has been shown to promote oncogenic Ras-induced transformation in Rat1 fibroblast cells (Izawa et al., 1998), thus suggesting Rho-kinase to play a negative role in oncogenic cells which is consistent with our previous study (Nakashima et al., 2010). Although we demonstrated that Rho-kinase regulates not only cell cycle progression (Nakashima et al., 2010), but also cell migration in colon cancer cells, further investigations are therefore required to clarify the precise role of Rho-kinase in cancer metastasis.

In conclusion, Rho-kinase negatively regulates cell migration at a point upstream of Akt/GSK-3β in colon cancer cells. This is the first report to show that Rho-kinase is involved in the negative regulation of colon cancer cell migration, thus providing important insight into the future development of potential therapeutic approaches for colon cancer patients. In other words, the regulation of Rho-kinase might be considered to be a new clinical target for cancer management, including the management of colon cancer.

Acknowledgments

We are very grateful to Ms. Yoko Kawamura for her skillful technical assistance. This work was supported in part by a Grant-in-Aid for Scientific Research (No. 22790639 to S.A.) from the Ministry of Education, Science, Sports and Culture of Japan.

References

Adachi, S., Nagao, T., Ingolfsson, H.I., Maxfield, F.R., Andersen, O.S., Kopelovich, L., Weinstein, I.B., 2007. The inhibitory effect of (−)-epigallocatechin gallate on activation of the epidermal growth factor receptor is associated with altered lipid order in HT29 colon cancer cells. Cancer Res. 67, 6493–6501.

Adachi, S., Nagao, T., To, S., Joe, A.K., Shimizu, M., Matsushima-Nishiwaki, R., Kozawa, O., Moriwaki, H., Maxfield, F.R., Weinstein, I.B., 2008. (−)-Epigallocatechin gallate causes internalization of the epidermal growth factor receptor in human colon cancer cells. Carcinogenesis 29, 1986–1993.

Adachi, S., Natsume, H., Yamauchi, J., Matsushima-Nishiwaki, R., Joe, A.K., Moriwaki, H., Kozawa, O., 2009a. p38 MAP kinase controls EGF receptor downregulation via phosphorylation at Ser1046/1047. Cancer Lett. 277, 108–113.

Adachi, S., Shimizu, M., Shirakami, Y., Yamauchi, J., Natsume, H., Matsushima-Nishiwaki, R., To, S., Weinstein, I.B., Moriwaki, H., Kozawa, O., 2009b. (−)-Epigallocatechin gallate downregulates EGF receptor via phosphorylation at Ser1046/1047 by p38 MAPK in colon cancer cells. Carcinogenesis 30, 1544–1552.

Bar-Sagi, D., Hall, A., 2000. Ras and Rho GTPases: a family reunion. Cell 103, 227–238.

Brew, C.T., Aronchik, I., Kosco, K., McCammon, J., Bjeldanes, L.F., Firestone, G.L., 2009. Indole-3-carbinol inhibits MDA-MB-231 breast cancer cell motility and induces stress fibers and focal adhesion formation by activation of Rho kinase activity. Int. J. Cancer 124, 2294–2302.

Burridge, K., 1981. Are stress fibres contractile? Nature 294, 691–692.

Burridge, K., Chrzanowska-Wodnicka, M., 1996. Focal adhesions, contractility, and signaling. Annu. Rev. Cell Dev. Biol. 12, 463–518.

Cross, D.A., Alessi, D.R., Cohen, P., Andjelkovich, M., Hemmings, B.A., 1995. Inhibition of glycogen synthase kinase-3 by insulin mediated by protein kinase B. Nature 378, 785–789.

Diaz-Rubio, E., 2006. Vascular endothelial growth factor inhibitors in colon cancer. Adv. Exp. Med. Biol. 587, 251–275.

Egeblad, M., Werb, Z., 2002. New functions for the matrix metalloproteinases in cancer progression. Nat. Rev. Cancer 2, 161–174.

Fritz, G., Just, I., Kaina, B., 1999. Rho GTPases are over-expressed in human tumors. Int. J. Cancer 81, 682–687.

Humphries, J.D., Wang, P., Streuli, C., Geiger, B., Humphries, M.J., Ballestrem, C., 2007. Vinculin controls focal adhesion formation by direct interactions with talin and actin. J. Cell Biol. 179, 1043–1057.

Itoh, K., Yoshioka, K., Akedo, H., Uehata, M., Ishizaki, T., Narumiya, S., 1999. An essential part for Rho-associated kinase in the transcellular invasion of tumor cells. Nat. Med. 5, 221–225.

Izawa, I., Amano, M., Chihara, K., Yamamoto, T., Kaibuchi, K., 1998. Possible involvement of the inactivation of the Rho–Rho-kinase pathway in oncogenic Ras-induced transformation. Oncogene 17, 2863–2871.

Joshi, B., Strugnell, S.S., Goetz, J.G., Kojic, L.D., Cox, M.E., Griffith, O.L., Chan, S.K., Jones, S.J., Leung, S.P., Masoudi, H., Leung, S., Wiseman, S.M., Nabi, I.R., 2008. Phosphorylated caveolin-1 regulates Rho/ROCK-dependent focal adhesion dynamics and tumor cell migration and invasion. Cancer Res. 68, 8210–8220.

Kerbel, R., Folkman, J., 2002. Clinical translation of angiogenesis inhibitors. Nat. Rev. Cancer 2, 727–739.

Matsui, T., Amano, M., Yamamoto, T., Chihara, K., Nakafuku, M., Ito, M., Nakano, T., Okawa, K., Iwamatsu, A., Kaibuchi, K., 1996. Rho-associated kinase, a novel serine/threonine kinase, as a putative target for small GTP binding protein Rho. EMBO J. 15, 2208–2216.

McHardy, L.M., Sinotte, R., Troussard, A., Sheldon, C., Church, J., Williams, D.E., Andersen, R.J., Dedhar, S., Roberge, M., Roskelley, C.D., 2004. The tumor invasion inhibitor dihydromotuporamine C activates RHO, remodels stress fibers and focal adhesions, and stimulates sodium-proton exchange. Cancer Res. 64, 1468–1474.

Nakashima, M., Adachi, S., Yasuda, I., Yamauchi, T., Kozawa, O., Moriwaki, H., 2010. Rho-kinase regulates negatively the epidermal growth factor-stimulated colon cancer cell proliferation. Int. J. Oncol. 36, 585–592.

Pellegrin, S., Mellor, H., 2007. Actin stress fibres. J. Cell Sci. 120, 3491–3499.

Pourgholami, M.H., Morris, D.L., 2008. Inhibitors of vascular endothelial growth factor in cancer. Cardiovasc. Hematol. Agents Med. Chem. 6, 343–347.

Ridley, A.J., Schwartz, M.A., Burridge, K., Firtel, R.A., Ginsberg, M.H., Borisy, G., Parsons, J.T., Horwitz, A.R., 2003. Cell migration: integrating signals from front to back. Science 302, 1704–1709.

Riento, K., Ridley, A.J., 2003. Rocks: multifunctional kinases in cell behaviour. Nat. Rev. Mol. Cell Biol. 4, 446–456.

Sahai, E., Ishizaki, T., Narumiya, S., Treisman, R., 1999. Transformation mediated by RhoA requires activity of ROCK kinases. Curr. Biol. 9, 136–145.

Sahai, E., Marshall, C.J., 2002. RHO-GTPases and cancer. Nat. Rev. Cancer 2, 133–142.

Salhia, B., Rutten, F., Nakada, M., Beaudry, C., Berens, M., Kwan, A., Rutka, J.T., 2005. Inhibition of Rho-kinase affects astrocytoma morphology, motility, and invasion through activation of Rac1. Cancer Res. 65, 8792–8800.

Shimokawa, H., Rashid, M., 2007. Development of Rho-kinase inhibitors for cardiovascular medicine. Trends Pharmacol. Sci. 28, 296–302.

Vecchiarelli-Federico, L.M., Cervi, D., Haeri, M., Li, Y., Nagy, A., Ben-David, Y., 2010. Vascular endothelial growth factor—a positive and negative regulator of tumor growth. Cancer Res. 70, 863–867.

Wozniak, M.A., Modzelewska, K., Kwong, L., Keely, P.J., 2004. Focal adhesion regulation of cell behavior. Biochim. Biophys. Acta 1692, 103–119.

Supplemental Material can be found at:
http://www.jbc.org/content/suppl/2011/08/12/M111.235473.DC1.html

⌘ *Author's Choice*

THE JOURNAL OF BIOLOGICAL CHEMISTRY VOL. 286, NO. 40, pp. 34800–34808, October 7, 2011

L-Tryptophan-mediated Enhancement of Susceptibility to Nonalcoholic Fatty Liver Disease Is Dependent on the Mammalian Target of Rapamycin*[S]

Received for publication, March 1, 2011, and in revised form, August 11, 2011 Published, JBC Papers in Press, August 12, 2011, DOI 10.1074/jbc.M111.235473

Yosuke Osawa[‡§1], Hiromitsu Kanamori[‡], Ekihiro Seki[¶], Masato Hoshi[‡], Hirofumi Ohtaki[‡], Yoichi Yasuda[§], Hiroyasu Ito[‡], Atsushi Suetsugu[§], Masahito Nagaki[§], Hisataka Moriwaki[§], Kuniaki Saito[‖], and Mitsuru Seishima[‡]

From the Departments of [‡]Informative Clinical Medicine and [§]Gastroenterology, Gifu University Graduate School of Medicine, Gifu 501-1194, Japan, the [¶]Department of Medicine, University of California, San Diego, School of Medicine, La Jolla, California 92093, and the [‖]Department of Human Health Science, Graduate School of Medicine and Faculty of Medicine, Kyoto University, Kyoto 606-8507, Japan

Nonalcoholic fatty liver disease is one of the most common liver diseases. L-Tryptophan and its metabolite serotonin are involved in hepatic lipid metabolism and inflammation. However, it is unclear whether L-tryptophan promotes hepatic steatosis. To explore this issue, we examined the role of L-tryptophan in mouse hepatic steatosis by using a high fat and high fructose diet (HFHFD) model. L-Tryptophan treatment in combination with an HFHFD exacerbated hepatic steatosis, expression of HNE-modified proteins, hydroxyproline content, and serum alanine aminotransaminase levels, whereas L-tryptophan alone did not result in these effects. We also found that L-tryptophan treatment increases serum serotonin levels. The introduction of adenoviral aromatic amino acid decarboxylase, which stimulates the serotonin synthesis from L-tryptophan, aggravated hepatic steatosis induced by the HFHFD. The fatty acid-induced accumulation of lipid was further increased by serotonin treatment in cultured hepatocytes. These results suggest that L-tryptophan increases the sensitivity to hepatic steatosis through serotonin production. Furthermore, L-tryptophan treatment, adenoviral AADC introduction, and serotonin treatment induced phosphorylation of the mammalian target of rapamycin (mTOR), and a potent mTOR inhibitor rapamycin attenuated hepatocyte lipid accumulation induced by fatty acid with serotonin. These results suggest the importance of mTOR activation for the exacerbation of hepatic steatosis. In conclusion, L-tryptophan exacerbates hepatic steatosis induced by HFHFD through serotonin-mediated activation of mTOR.

Nonalcoholic fatty liver disease (1) is a component of metabolic syndrome and a spectrum of liver disorders ranging from simple steatosis to nonalcoholic steatohepatitis (NASH),[2] which may cause liver cirrhosis and cancer. Hepatic steatosis occurs when the amount of imported and synthesized lipids exceeds the export or catabolism in hepatocytes. An excess intake of fat or carbohydrate is the main cause of hepatic steatosis. Changes in the dietary nutrient components also modulate hepatic steatosis. Nonalcoholic fatty liver disease patients consume 27% more meat protein from all types of meat (high fat meat, such as beef, liver, sausage, hot dog, and lamb, and low fat meat, such as chicken and turkey), which are sources of dietary tryptophan (2), as well as protein from fish, although less in comparison (3). These reports indicate that hepatic steatosis is also associated with the type of dietary protein consumed in addition to carbohydrate and fat.

Previous studies have shown involvement of amino acids in lipid metabolism in liver. L-Tryptophan is an essential aromatic amino acid and has important roles in protein synthesis and as a precursor of various bioactive compounds, such as serotonin, melatonin, kynurenine, nicotinamide adenine dinucleotide (NAD), and NAD phosphate (NADP). Although L-tryptophan has been widely used as an over-the-counter, natural remedy for depression, pain, insomnia, hyperactivity, and eating disorders (4), various adverse effects of excess tryptophan supplementation have been reported, including fatty liver (2). Oral administration or injection of L-tryptophan induces liver steatosis and increases hepatic fatty acid synthesis in rats (5–7). In mice, the expression of genes associated with the metabolism of L-tryptophan is significantly affected by a high fat diet (8), suggesting the involvement of L-tryptophan in lipid metabolism in the liver. In addition to L-tryptophan itself, its metabolites are also involved in the development of steatosis and steatohepatitis (9, 10).

L-Tryptophan is the precursor in two important metabolic pathways: serotonin synthesis and kynurenine synthesis. Serotonin is synthesized from L-tryptophan by the enzymes tryptophan hydroxylase and aromatic amino acid decarboxylase (AADC), and it regulates physiological functions in the hepatogastrointestinal tract (11). Tryptophan hydroxylase exists in the gastrointestinal tract (12), and AADC exists in the small intestine (13), appendix (13), and liver (14). In a NASH model

* This work was supported by Grants from the Takeda Science Foundation, Mitsubishi Pharma Research Foundation and by Ministry of Education, Culture, Sports, Science, and Technology of Japan Grants 21790657 and 23790787.

[S] The on-line version of this article (available at http://www.jbc.org) contains supplemental Figs. 1–3.

⌘ *Author's Choice*—Final version full access.

[1] To whom correspondence should be addressed: 1-1 Yanagido Gifu, 501-1194, Japan. Tel.: 81-58-230-6430; Fax: 81-58-230-6431; E-mail: osawa-gif@umin.ac.jp.

[2] The abbreviations used are: NASH, nonalcoholic steatohepatitis; AADC, aromatic amino acid decarboxylase; mTOR, mammalian target of rapamycin; HFHFD, high fat and high fructose diet; HNE, 4-hydroxy-2-nonenal; AMPK, AMP-activated protein kinase; ROS, reactive oxygen species; IDO, indoleamine 2,3-dioxygenase; HBSS, Hanks' balanced salt solution.

induced by a choline-methionine-deficient diet, serotonin-deficient tryptophan hydroxylase knock-out mice showed reduced hepatocellular injury and less severe inflammation (9). Liver steatosis induced by lymphocytic choriomeningitis virus infection is also serotonin-dependent (10), suggesting the involvement of serotonin in liver steatosis. Meanwhile, L-kynurenine is synthesized by indoleamine 2,3-dioxygenase (IDO) from L-tryptophan, which accounts for ~90% of tryptophan catabolism (4). L-Leucine is a branched amino acid and is involved in liver protein synthesis. L-Leucine deprivation induces liver steatosis in Gcn2 knock-out mice (15), whereas L-leucine supplementation reduced hepatic steatosis induced by high fat diet (16), suggesting a possible protective role of L-leucine against liver steatosis.

The mammalian target of rapamycin (mTOR) is a serine/threonine kinase and forms protein complexes that induce lipogenic gene expression (17). mTOR is activated in the livers of obese rats fed a high fat and high sucrose diet (18). The mTOR complex is important in the stimulation of lipogenesis in the liver (19), and the mTOR kinase inhibitor rapamycin reduces hepatic steatosis induced by a high fat diet (20). mTOR is also a master regulator of autophagy (21, 22), which is the process of degradation of intracellular components and distribution of nutrients under starving conditions. Upon food intake, amino acids and insulin inhibit autophagy through the mTOR and/or AKT-dependent pathways (23). Importantly, hepatic autophagy induces the breakdown of lipids stored in lipid droplets and regulates the lipid content in the liver (24, 25).

In the present study, we investigate the effects of L-tryptophan in hepatic steatosis. Our results suggest that L-tryptophan exacerbates hepatic steatosis induced by a high fat and high fructose diet (HFHFD) through serotonin and the activation of mTOR.

EXPERIMENTAL PROCEDURES

Animal Experiments—The experiments were conducted in accordance with the institutional guideline of Gifu University. Male wild-type C57BL/6J mice at 4 weeks of age were obtained from Japan SLC (Shizuoka, Japan). The mice were kept on a 12-h day/night cycle with free access to food and water. Hepatic steatosis was induced by feeding the animals HFHFD (a high fat diet (62.2% of calories from fat) (Oriental Yeast, Tokyo, Japan; HFD-60) and drinking water containing 30% fructose (Wako, Osaka, Japan)) for 8 weeks. Control mice were fed a normal diet (12.6% of calories from fat) (CLEA Japan, Tokyo, Japan; CE-2) with plain water. L-Tryptophan or L-leucine (Sigma-Aldrich) was administered in the drinking water at a concentration of 0.25% (w/v) (L-tryptophan) and 1% (L-leucine), respectively, at a dose of ~400 and 1600 mg/kg/day. Control animals were treated with bovine serum albumin (BSA) (Wako, Osaka, Japan) in the drinking water at a concentration of 0.25%. At the end of the study period, the animals were deprived of food for 18 h, and the drinking water was changed to plain water without fructose, L-tryptophan, or L-leucine. After recording body weight, the mice were anesthetized and humanely killed by withdrawal of blood. The liver was immediately removed and washed in ice-cold phosphate-buffered saline (PBS). Subsequently, weight measurements of liver were taken, and a part of the dissected liver tissue was frozen in liquid nitrogen. Serum alanine aminotransaminase was measured using an automatic analyzer (JEOL Ltd., Tokyo, Japan; BM2250).

Cell Culture and Treatments—Male wild-type C57BL/6J mice (8–12 weeks old) were anesthetized, and then hepatocytes were isolated by a nonrecirculating *in situ* collagenase perfusion of livers cannulating through the inferior vena cava as described previously (26) with minor modifications. Livers were first perfused *in situ* with 0.5 mM EGTA containing calcium-free salt solution, followed by perfusion with solution containing collagenase (0.65 mg/ml) (Wako). The livers were then gently minced on a Petri dish and filtered with nylon mesh (Tokyo Screen, Tokyo, Japan; N-No.270T). Hepatocytes were washed three times with Hanks' balanced salt solution (HBSS). Cell viability was consistently >90%, as determined by trypan blue exclusion. Cells were plated on 6-well plates (1×10^6 cells/well) coated with rat tail collagen type I (BD Biosciences; BioCoat) in Waymouth medium (Invitrogen) containing 10% fetal bovine serum supplemented with penicillin and streptomycin (Invitrogen) for 4 h. Hc hepatocytes (normal human fetal hepatocytes) and cell culture medium (CS-C complete) was obtained from Applied Cell Biology Research Institute and Cell Systems, respectively. Hc hepatocytes were cultured in CS-C complete medium supplemented with penicillin and streptomycin and maintained at 37 °C in a 5% CO_2 atmosphere. Cells were plated on 6-well plates (1×10^6 cells/well) and were incubated in the medium for 24 h. Primary cultured mouse hepatocytes and Hc hepatocytes were then washed twice with PBS, and the medium was changed to serum-free RPMI 1640 containing 0.5% BSA and the antibiotics. After a 1-h incubation, the cells were treated with or without 100 μM serotonin (Sigma-Aldrich) and/or fatty acid mixture (100 μM linoleic acid and 100 μM oleic acid) (Sigma-Aldrich; L9655) for 2 h for protein extraction and 18 h for Oil Red O staining and triglyceride measurement. When necessary, the cells were pretreated with 100 nM rapamycin (Sigma-Aldrich) dissolved in DMSO for 30 min before treatment with serotonin and/or fatty acids. For induction of autophagy in Hc hepatocytes, cells were washed twice with PBS, and the medium was changed to HBSS with or without rapamycin. After a 0.5-h incubation, the cells were treated with or without serotonin and incubated for an additional 3 h. For control, the cells were cultured in RPMI1640 medium containing 10% FBS.

Histological Analysis—The livers were fixed with 10% formalin, and paraffin blocks were sectioned and stained with hematoxylin and eosin (H&E). Collagen deposition was stained with Sirius Red (saturated picric acid containing 0.1% DirectRed 80 and 0.1% FastGreen FCF) as reported previously (27). For frozen liver sections, the fixed livers were soaked in 15% sucrose in PBS for 12 h following with 30% sucrose for 24 h at 4 °C under constant agitation and were then embedded in OTC compound. For 4-hydroxy-2-nonenal (HNE) staining, the frozen liver sections were cut at a thickness of 5 μm with a cryostat and stained with anti-HNE antibody (Alpha Diagnostic International; HNE11-S).

Oil Red O Staining—For lipid droplet staining, the frozen liver sections were cut at a thickness of 5 μm using a cryostat

and were subsequently stained with Oil Red O (Muto Pure Chemicals, Tokyo, Japan) working solution. Hematoxylin was used for counterstaining. For cells, the Hc hepatocytes were fixed with 10% formalin and then stained with Oil Red O.

Measurement of Triglyceride—Triglyceride content in the serum, liver tissue, and cells was measured using a triglyceride E-test kit (Wako). For liver tissues, the frozen liver tissues were homogenized in PBS, and methanol was added to the lysate. For cells, the Hc hepatocytes were washed with PBS and scraped with methanol. The lipids were extracted by the Bligh and Dyer method.

Western Blot—For the preparation of total cell proteins, cells or frozen liver tissues were sonicated in radioimmunoprecipitation assay buffer (50 mM Tris-HCl, pH 7.5, 150 mM NaCl, 10 mM EGTA, 1% Triton-X, 0.1% SDS) containing protease inhibitors and phosphatase inhibitors (Roche Applied Science; PhosSTOP phosphatase inhibitor mixture and Complete protease inhibitor mixture tablets). The proteins were separated by SDS-PAGE and were electrophoretically transferred onto nitrocellulose membrane. The membranes were first incubated with the primary antibodies, anti-HNE, phospho-mTOR (Ser^{2448}) (Cell Signaling Technology; catalog no. 2971), mTOR (Cell Signaling; catalog no. 2972), phospho-p70S6K (Thr^{389}) (Cell Signaling; catalog no. 9234), p70S6K (Cell Signaling; catalog no. 2708), phospho-AKT (Ser^{473}) (Cell Signaling; catalog no. 9271), AKT (Cell Signaling; catalog no. 9272), phospho-AMP-activated protein kinase α (AMPKα) (Thr^{172}) (Cell Signaling; catalog no. 2531), AMPKα (Cell Signaling; catalog no. 2603), p62 (MBL; PM045), and glyceraldehyde 3-phosphate dehydrogenase (GAPDH) (Cell Signaling; catalog no. 2118) antibodies. Then the membranes were incubated with the horseradish peroxidase (HRP)-coupled secondary antibodies (Santa Cruz Biotechnology, Inc., Santa Cruz, CA). Detection was performed with ImmunoStar LD (Wako), and the protein bands were quantified by densitometry using the ImageJ program (National Institutes of Health, Bethesda, MD).

Quantitative Real-time RT-PCR—Extracted RNA from the liver was reverse-transcribed by a high capacity cDNA reverse transcription kit (Applied Biosystems), and quantitative real-time PCR was performed using SYBR premix Ex Taq (Takara, Shiga, Japan) with ABI Prism 7000 (Applied Biosystems). The changes were normalized based on 18 S rRNA. PCR primer sequences were listed as follows: transforming growth factor (TGF)-β1, GTGGAAATCAACGGGATCAG (forward) and ACTTCCAACCCAGGTCCTTC (reverse); collagen α1(I), TAGGCCATTGTGTATGCAGC (forward) and ACATGTTCAGCTTTGTGGACC (reverse); 18 S, AGTCCCTGCCCTTTGTACACA (forward) and CGATCCGAGGGCCTCACTA (reverse).

Hydroxyproline Measurement—Hydroxyproline was measured for assessment of collagen content. The extracted liver protein was hydrolyzed in 6 M HCl (100 °C, 24 h). The samples were neutralized with LiOH, and hydroxyproline content was measured using a high performance liquid chromatographic analyzer (Jasco, Hitachi, and Shimazu).

Recombinant Adenoviruses—The recombinant replication-deficient adenoviruses Ad5IDO and Ad5AADC, expressing IDO and AADC, respectively, were constructed by the AdEasy^{TM} adenoviral vector system (Stratagene) as described previously (28). Briefly, the full length of mouse IDO and AADC cDNA was amplified by PCR with the following primers: IDO, ATAGGTACCGCCGCCATGGCACTCAGTAAAATATCTCCTACAGAAGGTTC (forward) and ATACTCGAGCTAAGGCCAACTCAGAAGAGCTTTCTCGGTTGTATCTTT (reverse); AADC, ATAGGTACCGCCGCCATGGATTCCCGTGAATTCCGGAGGAGAGGCAAGGA (forward) and ATACTCGAGTCATTCTTTCTCTGCCCTCAGCACACTGCTTGCTAG (reverse). The cDNA fragment was subcloned into pAdTrack-CMV adenoviral vector. The plasmid DNA was prepared by the alkaline lysis method and transfected into BJ5183-AD-1 electroporation-competent cells. The virus was grown in 293 cells and purified by banding twice on CsCl gradients and then dialyzed and stored at −20 °C. Mice were infected with the adenoviruses (5×10^8 pfu/mouse) by intravenous injection 7 days before sacrifice. Gene expressions by the adenovirus vectors were preferentially observed in the liver (mainly in the hepatocytes) but not in the muscle and adipose tissue (data not shown), as reported previously (28, 29). The adenovirus Ad5GFP, which expresses green fluorescent protein, was used as infection control.

Measurement of L-Tryptophan, L-Kynurenine, and Serotonin—Serum L-tryptophan and L-kynurenine were measured by HPLC with a spectrophotometric detector (Tosoh, Tokyo, Japan; Tosoh ultraviolet-8000) or fluorescence spectrometric detector (Hitachi, Tokyo, Japan) as described in a previous report (30). Serum serotonin was measured by Serotonin FAST ELISA (DRG International, Marburg, Germany).

Statistical Analysis—The results shown are representative of at least three independent experiments. Data are expressed as mean ± S.D. from at least four independent experiments. Data between groups were analyzed by Student's *t* test. A value of $p < 0.05$ was considered statistically significant.

RESULTS

L-Tryptophan Exacerbates Hepatic Steatosis and Fibrosis—Hepatic steatosis was induced by HFHFD in mice. The HFHFD caused an increase in body weight (Fig. 1*A*) and induced hepatic steatosis (Fig. 1, *B* and *C*), whereas the body/liver weight ratio was decreased (Fig. 1*A*). To examine the effect of L-tryptophan on hepatic steatosis, mice fed with HFHFD were treated with L-tryptophan or BSA. To confirm the specific effect of L-tryptophan, L-leucine was used as a control amino acid. Although L-tryptophan alone did not induce hepatic steatosis, a combination of L-tryptophan and HFHFD exacerbated hepatic steatosis and reversed the reduction of the body/liver weight ratio (Fig. 1, *A–C*) without changing food and water intake, blood glucose, or serum triglyceride levels (data not shown). L-Tryptophan treatment with HFHFD significantly increased serum alanine aminotransaminase levels (Fig. 2*A*) and formation of reactive oxygen species (ROS) as assessed by expression of HNE-modified proteins (Fig. 2*B*). Although expression of fibrogenic gene collagen α1(I), but not TGF-β, was up-regulated in HFHFD-fed animals (Fig. 2*C*), L-tryptophan treatment further increased the expression of TGF-β and collagen α1(I) in the livers of mice treated with HFHFD (Fig. 2*C*).

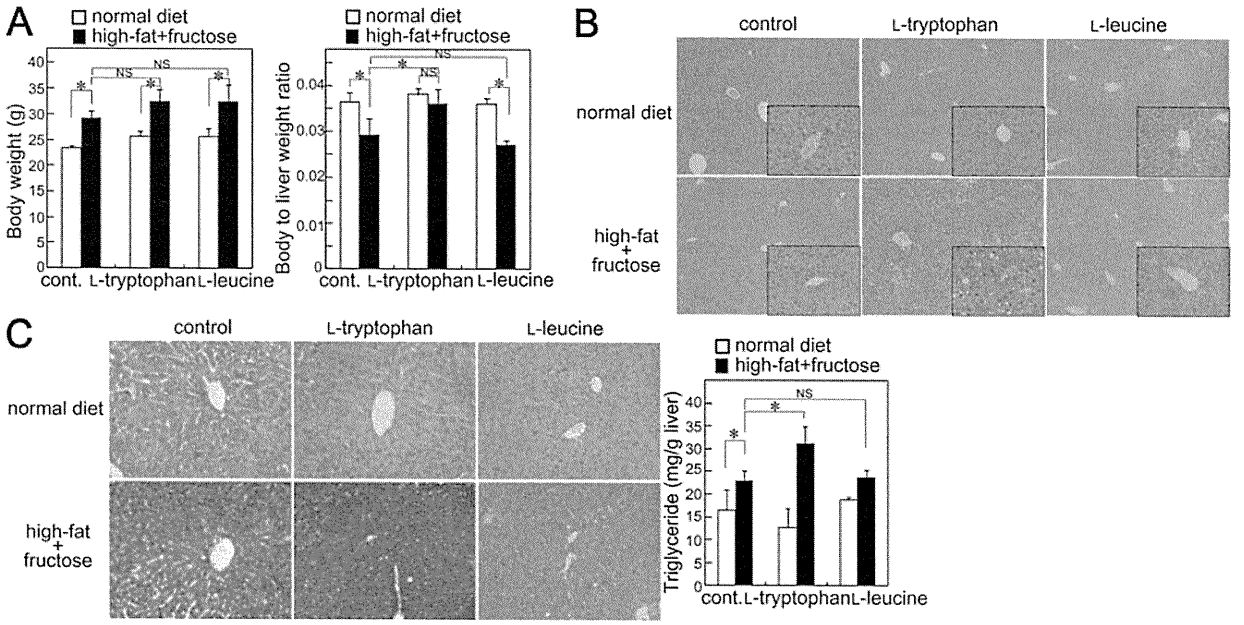

FIGURE 1. **L-Tryptophan exacerbates hepatic steatosis.** Mice were fed a normal diet or HFHFD supplemented with or without L-tryptophan or L-leucine for 8 weeks. The animals were humanely killed under fasting conditions (18 h of food deprivation). *A*, body weight (*left*) and liver weight were measured, and the body/liver weight ratio was calculated (*right*). *B*, liver sections were stained with H&E (original magnification, ×100 and ×400 (*insets*)). *C*, hepatic lipid content was assessed by Oil Red O staining (*left*; original magnification, ×200) and triglyceride measurement (*right*). Results shown are representative of at least three independent experiments. Data are means ± S.D. from at least four independent experiments. *, $p < 0.05$. *NS*, not significant.

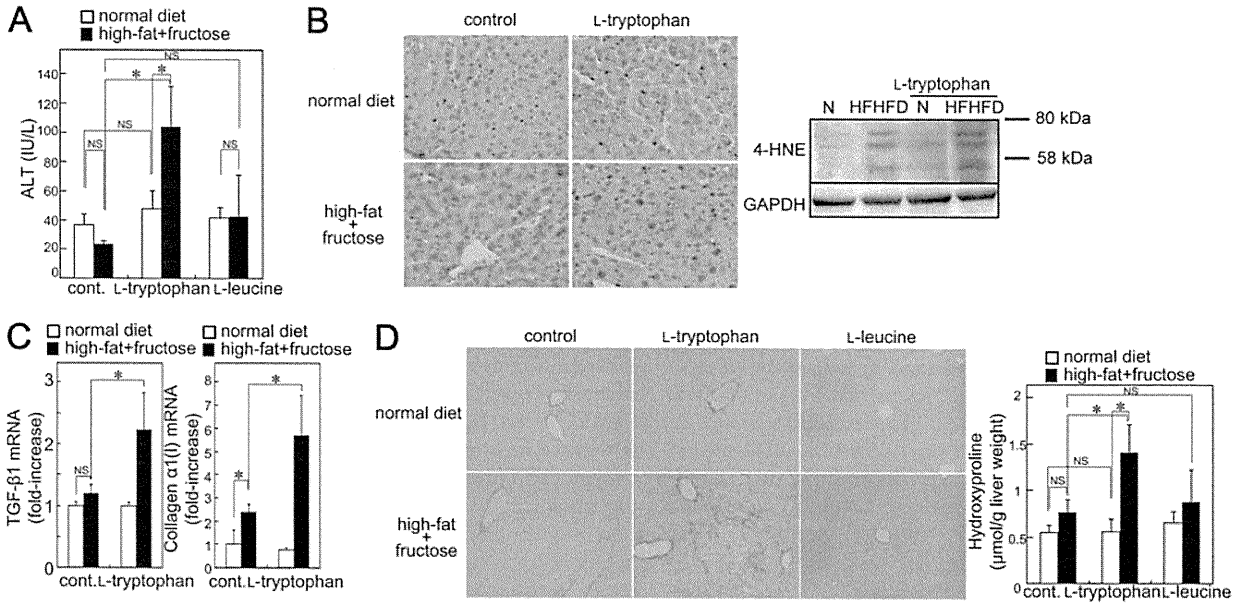

FIGURE 2. **L-Tryptophan induces hepatic fibrosis in steatotic liver.** Mice were fed a normal diet (*N*) or HFHFD supplemented with or without L-tryptophan or L-leucine for 8 weeks. *A*, serum alanine aminotransaminase levels were compared. *B*, expression of HNE-modified proteins in liver tissue was examined by immunohistochemistry (*left*; original magnification, ×400). Protein extracts from liver tissue were subjected to SDS-PAGE, and immunoblotting was performed with anti-HNE and GAPDH antibodies (*right*). *C*, mRNA levels of TGF-β1 and collagen α1(I) in liver tissue were determined by quantitative real-time RT-PCR. *D*, collagen deposition was assessed by Sirius Red staining (*left*; original magnification, ×200) and measurement of hydroxyproline content (*right*). Results shown are representative of at least three independent experiments. Data are means ± S.D. from at least four independent experiments. *, $p < 0.05$. *NS*, not significant.

Interestingly, although a combination of the L-tryptophan and HFHFD treatments induced liver fibrosis, neither treatment alone induced liver fibrosis (Fig. 2*D*). In contrast, L-leucine treatment did not enhance HFHFD-mediated steatosis, liver injury, and fibrosis (Fig. 2, *A* and *D*). These results suggest that the L-tryptophan increases hepatic steatosis, ROS

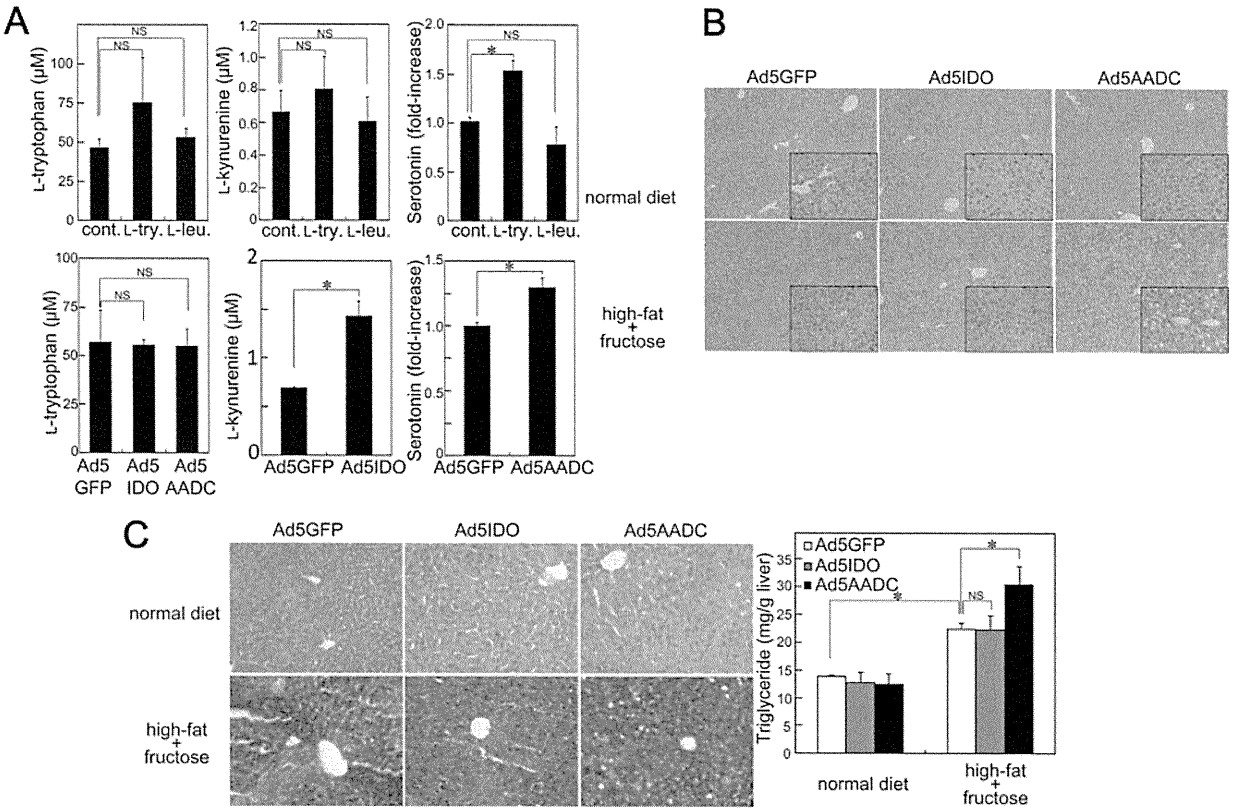

FIGURE 3. **Exogenous introduction of AADC aggravates hepatic steatosis.** *A*, mice were fed a normal diet supplemented with or without L-tryptophan or L-leucine for 8 weeks (*top panels*). Mice were infected with Ad5GFP, Ad5IDO, or Ad5AADC (5×10^8 pfu/mouse) and were humanely killed 7 days after the adenoviral infection (*bottom panels*). Serum L-tryptophan, L-kynurenine, and serotonin levels were measured. *B*, mice were fed with a normal diet or HFHFD for 8 weeks. The mice were infected with or without Ad5GFP, Ad5IDO, or Ad5AADC (5×10^8 pfu/mouse) at the end of 7-week period and were humanely killed on 7 days after the adenoviral infection under fasting conditions (18 h of food deprivation). Liver sections were stained with H&E (original magnification, ×100 and ×400 (insets)). *C*, hepatic lipid content was assessed by Oil Red O staining (*left*; original magnification, ×200) and triglyceride measurement (*right*). Results shown are representative of at least three independent experiments. Data are means ± S.D. from at least four independent experiments. *, $p < 0.05$. *NS*, not significant.

production, liver injury, and fibrosis induced by excessive fat and fructose intake.

Exogenous AADC or Serotonin Aggravates Hepatic Steatosis—To investigate the mechanisms by which L-tryptophan enhances HFHFD-induced hepatic steatosis, serum levels of L-tryptophan and its metabolites L-kynurenine and serotonin were measured. L-Tryptophan intake did not affect serum levels of L-tryptophan or L-kynurenine (Fig. 3*A*). Importantly, serum serotonin levels were significantly increased by treatment with L-tryptophan but not by L-leucine treatment (Fig. 3*A*). Adenoviral AADC introduction also increased serum serotonin levels without decreasing L-tryptophan levels (Fig. 3*A*) in addition to increased hepatic steatosis and triglyceride levels in HFHFD-fed animals (Fig. 3, *B* and *C*). Ad5IDO-infected mice with increased levels of serum L-kynurenine showed similar levels of lipid accumulation compared with control adenovirus-infected mice (Fig. 3*A*). This indicates synthesis of serotonin but not kynurenine as a crucial component of hepatic steatosis enhanced by L-tryptophan treatment. Subsequently, we investigated the effect of serotonin on lipid accumulation *in vitro* using primary cultured hepatocytes and Hc hepatocytes. The serotonin treatment in addition to fatty acid (linoleic acid and oleic acid) amplified the effects, such as accumulation of lipid droplets and increase of triglycerides, seen in fatty acid-treated cells (Fig. 4, *A* and *B*). In contrast, serotonin alone did not induce lipid accumulation. These results indicate that serotonin exacerbates lipid accumulation in hepatocytes. This further suggests that L-tryptophan treatment aggravates hepatic steatosis through serotonin.

mTOR Activation Is Crucial for L-Tryptophan-mediated Exacerbation of Hepatic Steatosis—To investigate the mechanisms underlying the effect of L-tryptophan on hepatic steatosis, we assessed the activation of mTOR, AKT, and AMPK, which are key molecules in the regulation of lipogenesis (17, 28). L-Tryptophan treatment induced phosphorylation of mTOR and p70S6K, a downstream target of mTOR in mouse livers under food-deprived conditions (Fig. 5*A* and supplemental Fig. 1*A*). In contrast, L-leucine treatment did not affect phosphorylation of mTOR or p70S6K. Although the HFHFD alone increased AKT and decreased AMPK phosphorylation, L-tryptophan or L-leucine treatment did not affect AKT or AMPK phosphorylation. Adenoviral AADC introduction also increased the phosphorylation of mTOR and p70S6K (Fig. 5*B* and supplemental Fig. 1*A*), suggesting that increased serotonin levels induce mTOR and p70S6K phos-

phorylation. Importantly, serotonin treatment increased mTOR and p70S6K phosphorylation in both primary cultured mouse hepatocytes and Hc hepatocytes (Fig. 6, *A* and *B*, and supplemental Fig. 1*B*). These results led to the hypothesis that mTOR activation contributes to the L-tryptophan/serotonin-mediated exacerbation of hepatic steatosis. Therefore, we investigated the role of serotonin-mediated mTOR activation by inhibiting mTOR activation using rapamycin, a potent inhibitor of mTOR. Rapamycin successfully inhibited the serotonin-mediated phosphorylation of mTOR and p70S6K (Fig. 6, *A* and *B*, and supplemental Fig. 1*B*) and lipid accumulation (Fig. 6, *C* and *D*). The requirement of mTOR activation in L-tryptophan/serotonin signaling for hepatic steatosis was also examined *in vivo*. Treatment with rapamycin significantly inhibited the phosphorylation of mTOR and p70S6K induction by L-tryptophan in mouse livers (supplemental Fig. 2*A*). Normal body weight increase following HFHFD was also diminished in rapamycin-treated mice (supplemental Fig. 2*B*) without change in the food or water intake (data not shown), as reported previously (20). Moreover, rapamycin treatment attenuated hepatic steatosis (supplemental Fig. 2, *C* and *D*), levels of alanine aminotransaminase (supplemental Fig. 2*E*), hepatic expression of HNE-modified proteins (supplemental Fig. 2*F*), and hepatic hydroxyproline content (supplemental Fig. 2*G*) in HFHFD and L-tryptophan-treated mice. These results suggest requirement of mTOR activation for the exacerbation of hepatic steatosis, liver damage, ROS formation, and liver fibrosis in the HFHFD- and L-tryptophan-treated animals.

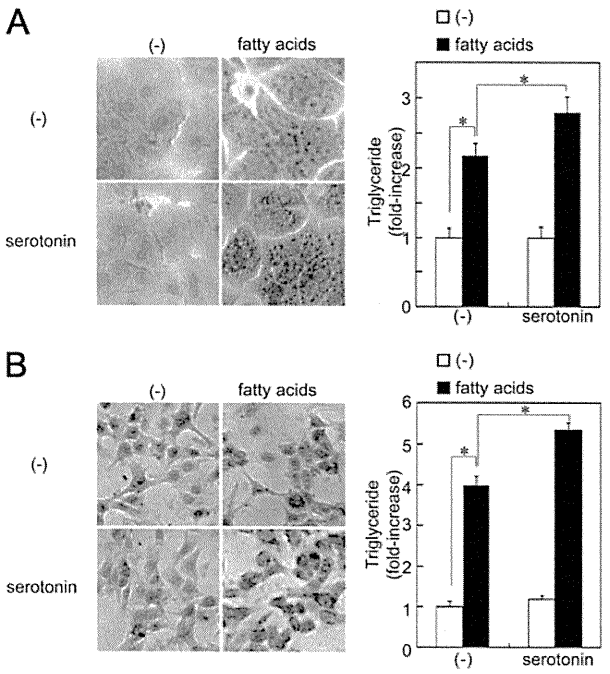

FIGURE 4. **Serotonin exacerbates lipid accumulation in hepatocytes.** Primary cultured mouse hepatocytes (*A*) or Hc hepatocytes (*B*) were treated with or without fatty acids (100 μM linoleic acid and 100 μM oleic acid) in the presence or absence of 100 μM serotonin for 18 h. Lipid droplets were assessed by Oil Red O staining (*left panels*; original magnification, ×400). Triglyceride levels in hepatocytes were determined (*right panel*). Results shown are representative of at least three independent experiments. Data are means ± S.D. from at least four independent experiments. *, $p < 0.05$.

Hepatic Autophagy Is Suppressed by L-Tryptophan/Serotonin Treatment—A high fat diet inhibits hepatic autophagy in mice (31), and the inhibition of autophagy in cultured hepatocytes and mouse livers showed an increase in triglyceride storage (25), suggesting that inhibited hepatic autophagy is involved in liver steatosis. Because mTOR is a master regulator of autophagy (21, 22) and an L-tryptophan/serotonin activated mTOR (Figs. 5 and 6), we examined the role of L-tryptophan/serotonin in hepatic autophagy by assessing LC3 aggregation and p62 degradation, which are hallmarks of autophagy. Although food deprivation induced LC3 aggregation and p62 degradation in the liver (supplemental Fig. 3*A*), HFHFD treatment suppressed the LC3 aggregation and p62 degradation (Fig. 7), indicating that autophagy is induced by cellular starvation but inhibited in steatotic hepatocytes. We found that L-tryptophan treatment suppressed LC3 aggregation and p62 degradation in mice with food deprivation (supplemental Fig. 3*A*), suggesting the inhibition of hepatic autophagy by L-tryptophan. Similarly, exogenous AADC expression, but not GFP or IDO expression, also suppressed LC3 aggregation and p62 degradation after food deprivation (supplemental Fig. 3*B*), suggesting that serotonin synthesis by introduction of AADC inhibits fasting-induced autophagy. As described above (supplemental Fig. 2), rapamycin improved hepatic steatosis. Similarly, rapa-

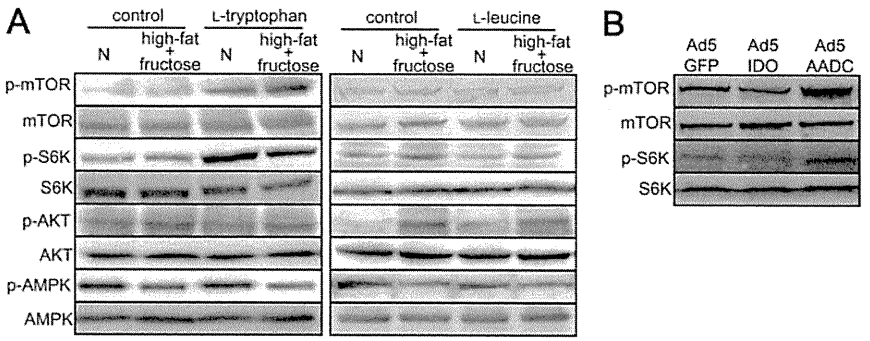

FIGURE 5. **L-Tryptophan induces mTOR activation.** *A*, mice were fed with normal diet (*N*) or HFHFD supplemented with or without L-tryptophan or L-leucine for 8 weeks. *B*, mice were infected with Ad5GFP, Ad5IDO, or Ad5AADC (5×10^8 pfu/mouse) and were humanely killed on 7 days after the adenoviral infection. Protein extracts from liver tissue or hepatocytes were subjected to immunoblot for phospho-mTOR, mTOR, phospho-p70S6K, p70S6K, phospho-AKT, AKT, phospho-AMPK, or AMPK, respectively. Results shown are representative of at least three independent experiments. The results of densitometric analysis are shown in supplemental Fig. 1*A*.

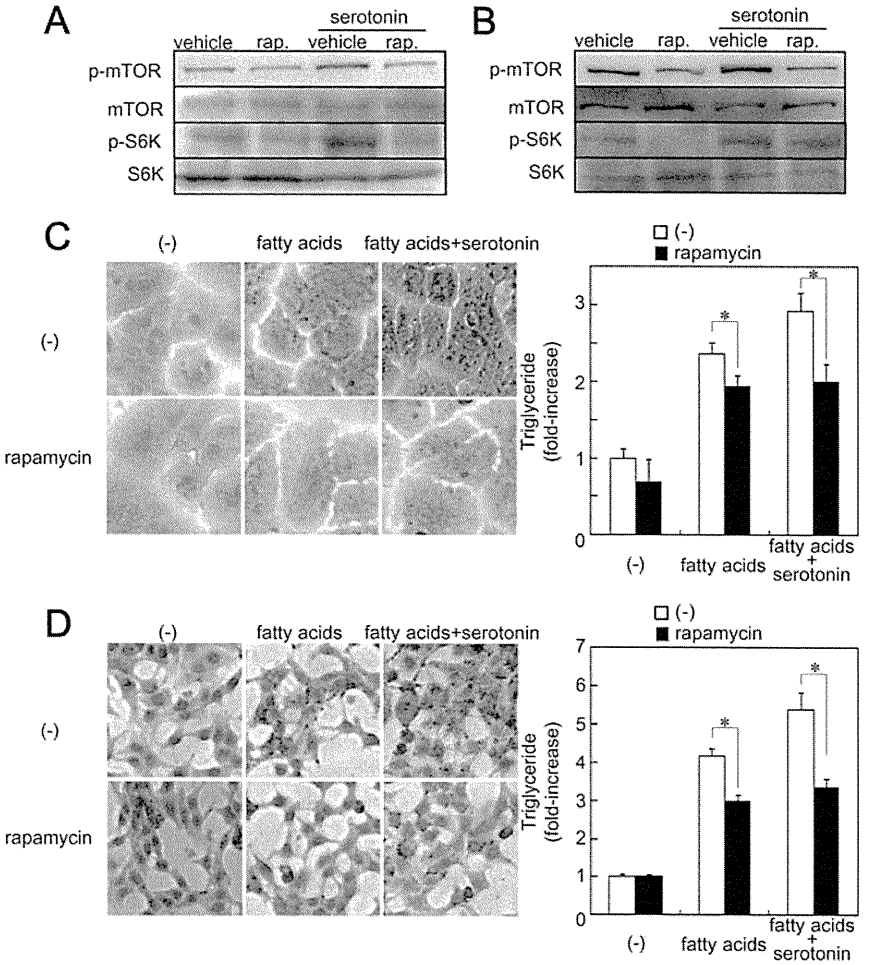

FIGURE 6. **Rapamycin improves lipid accumulation in hepatocytes.** Primary cultured mouse hepatocytes (*A* and *C*) or Hc hepatocytes (*B* and *D*) were pretreated with or without 100 nM rapamycin for 30 min. *A* and *B*, the hepatocytes were treated with or without 100 μM serotonin for 2 h. Protein extracts from hepatocytes at 2 h after the serotonin treatment were subjected to immunoblot for phospho-mTOR, mTOR, phospho-p70S6K, and p70S6K, respectively. *C* and *D*, the hepatocytes were treated with or without fatty acids (100 μM linoleic acid and 100 μM oleic acid) in the presence or absence of 100 μM serotonin for 18 h. Lipid droplets were assessed by Oil Red O staining (*left panels*; original magnification, ×400). Triglyceride levels in hepatocytes were determined (*right panel*). Results shown are representative of at least three independent experiments. Data are means ± S.D. from at least four independent experiments. *, $p < 0.05$. The results of densitometric analysis are shown in supplemental Fig. 1*B*.

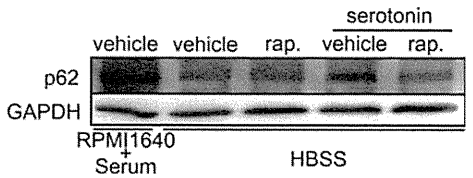

FIGURE 7. **Serotonin inhibits p62 degradation.** Hc hepatocytes were pretreated with or without rapamycin in HBSS. After 0.5 h of incubation, the cells were treated with or without serotonin and incubated for an additional 3 h. As a control, the cells were cultured in RPMI1640 medium containing FBS. Protein extracts were subjected to immunoblot for p62 or GAPDH, respectively. Results shown are representative of at least three independent experiments.

mycin treatment induced LC3 aggregation and p62 degradation in L-tryptophan-treated mice. These results demonstrated that inhibition of mTOR by rapamycin reversed L-tryptophan-mediated inhibition of autophagy (supplemental Fig. 3*C*), suggesting the ability of L-tryptophan to inhibit autophagy through mTOR. Subsequently, we examined whether serotonin suppresses autophagy through mTOR activation in hepatocytes. Hc hepatocytes were cultured in HBSS, amino acid-free conditions, for autophagy induction, and we assessed the levels of p62 (Fig. 7). In the Hc hepatocytes with starvation, autophagy was induced, as demonstrated by p62 degradation. Starvation-induced p62 degradation was inhibited by serotonin treatment, whereas rapamycin treatment induced p62 degradation in serotonin-treated cells. These results suggest that the inhibitory effects of L-tryptophan and serotonin on autophagy were reversed by inhibition of mTOR. This further suggests the suppression of hepatic autophagy as one of the possible mechanisms by which hepatic steatosis is enhanced by L-tryptophan/serotonin.

DISCUSSION

The present study examined the contribution of L-tryptophan to hepatic steatosis. L-Tryptophan has been reported to

induce hepatic steatosis in rats (5, 6). However, a conflicting report indicates that L-tryptophan does not cause fatty liver (32). In the present study, L-tryptophan treatment did not induce hepatic steatosis under normal diet conditions but had a stimulatory effect on hepatic steatosis when combined with HFHFD. HFHFD increased body weight, whereas the body/liver weight ratio was decreased. This indicates the accumulation of excess fat as body fat rather than visceral fat. In contrast, the combination of L-tryptophan and HFHFD exacerbated hepatic steatosis and reversed reduction of the body/liver weight ratio, which suggests that L-tryptophan induces accumulation of excess fat as visceral fat. This further suggests the overconsumption of L-tryptophan-rich protein (*e.g.* milk, cheese, meat, and sausage) as a possible cause of an aggravation of hepatic steatosis induced by excessive intake of fat and carbohydrate.

In addition to its role as a substrate for protein synthesis, L-tryptophan is the precursor of kynurenine and serotonin. Exogenous introduction of IDO by adenovirus or intraperitoneal administration of the IDO inhibitor 1-methyl-DL-tryptophan did not affect the lipid content of the liver (data not shown), suggesting a minor role of the kynurenine synthesis pathway in L-tryptophan-mediated biology on hepatic steatosis.

Adenoviral AADC introduction increased serum serotonin levels without decreasing L-tryptophan levels. In the serotonin synthesis pathway, a part of L-tryptophan is converted to 5-hydroxy-L-tryptophan by tryptophan hydroxylase and further converted to serotonin by AADC. L-Tryptophan is mostly used as material for protein synthesis, and a part of L-tryptophan may be used for serotonin synthesis. Thus, AADC increased serotonin levels without any changes in serum levels of tryptophan. Both L-tryptophan treatment and exogenous introduction of AADC increased lipid accumulation in the livers of mice fed with HFHFD. Moreover, an *in vitro* experiment using hepatocytes demonstrated that fatty acid-induced accumulation of lipid droplets and triglyceride synthesis were further increased by the treatment of serotonin. These findings suggest that serotonin is an essential component in the exacerbation of hepatic steatosis in L-tryptophan-treated mice.

Liver injury and fibrosis were induced in mice treated with HFHFD and L-tryptophan. Treatment with rapamycin attenuated liver injury and fibrosis with reduced hepatic steatosis. ROS formation plays a central role in the pathogenesis of liver damage and fibrosis in NASH (33). We found that L-tryptophan treatment significantly increased ROS production in the steatotic livers, which may be one of the central mechanisms by which L-tryptophan aggravates liver damage and fibrosis. A previous report demonstrated that serotonin-deficient tryptophan hydroxylase knock-out mice have reduced ROS, inflammation, and hepatocellular injury in NASH induced by a choline-methionine-deficient diet (9). This report is consistent with the other reports demonstrating that serotonin induces oxidative stress and mitochondrial toxicity in NASH (9). In addition, tryptophan itself can also induce oxidative stress (34). In the present study, L-tryptophan induced ROS formation in the steatotic livers, suggesting that L-tryptophan-mediated ROS formation requires lipid accumulation. In rat cerebral cortex tissue, L-tryptophan treatment reduces total radical-trapping antioxidant potential, total antioxidant reactivity, and glutathione levels (35). This suggests that suppression of antioxidants by L-tryptophan may one of the mechanisms of increased ROS formation in steatotic livers.

L-Tryptophan treatment increased hepatic mTOR phosphorylation after food deprivation (Fig. 5). Inhibition of mTOR by rapamycin reversed hepatic steatosis enhanced by L-tryptophan, suggesting that mTOR activation is a key for L-tryptophan-mediated exacerbation of hepatic steatosis. AKT is an upstream kinase in mTOR signaling (36) and is a key molecule for glucose and lipid metabolism. Sustained AKT activation in PTEN (phosphatase and tensin homolog on chromosome 10)-deleted livers induces fatty liver (37). In our model, food intake increased AKT and mTOR phosphorylation in mouse livers (data not shown). The HFHFD induced AKT phosphorylation but not mTOR phosphorylation under food-deprived conditions. In contrast, L-tryptophan treatment did not affect AKT phosphorylation, suggesting that L-tryptophan-mediated mTOR activation is not induced by AKT activation.

It has been reported that leucine regulates mTOR signaling, and acute administration of leucine induces phosphorylation of S6K in the liver (38) and the adipose tissue (39). Thus, we had to examine the specificity of the effect by L-tryptophan. We used L-leucine as a control amino acid. In contrast to L-tryptophan, phosphorylation of mTOR and S6K was not observed after L-leucine treatment. Our data are consistent with another previous report showing that chronic administration of leucine does not change S6K phosphorylation in the livers of rats (40) and neonatal pigs (41). Thus, L-tryptophan, but not L-leucine, induces activation of mTOR signaling.

Autophagy is activated by nutrient deprivation but inhibited by amino acids and/or released insulin after food intake (23). LC3 aggregation and p62 degradation, markers for autophagy, were induced in the liver after fasting. In contrast, the levels of LC3 aggregation and p62 degradation were suppressed in mice fed with HFHFD. This may be explained by hyperinsulinemia in mice fed a high fat diet (31). We also found L-tryptophan to have an inhibitory effect on hepatic autophagy (supplemental Fig. 3). Because L-tryptophan did not increase serum insulin level (data not shown), the effect of L-tryptophan may not be due to hyperinsulinemia. Instead, serotonin production was found to be crucial for L-tryptophan-mediated mTOR activation in the liver (Fig. 5). In combination with the previous report that serotonin treatment suppresses autophagy in hepatocellular carcinoma cells (42), our data suggest that L-tryptophan suppresses hepatic autophagy through serotonin production and mTOR activation. Because mTOR strongly inhibits autophagy and autophagy is important for regulating the breakdown of stored lipids (25), hepatic autophagy inhibited by L-tryptophan may be one of the mechanisms in the aggravation of hepatic steatosis.

In conclusion, L-tryptophan exacerbates hepatic steatosis by producing serotonin that activates mTOR signaling in mice fed with HFHFD. In addition to a calorie-restricted diet, targeting L-tryptophan may become a new therapeutic strategy for nonalcoholic fatty liver disease patients.

REFERENCES

1. Angulo, P. (2002) *N. Engl. J. Med.* **346,** 1221–1231
2. Sainio, E. L., Pulkki, K., and Young, S. N. (1996) *Amino Acids* **10,** 21–47
3. Zelber-Sagi, S., Nitzan-Kaluski, D., Goldsmith, R., Webb, M., Blendis, L., Halpern, Z., and Oren, R. (2007) *J. Hepatol.* **47,** 711–717
4. Richard, D. M., Dawes, M. A., Mathias, C. W., Acheson, A., Hill-Kapturczak, N., and Dougherty, D. M. (2009) *Int. J. Tryptophan. Res.* **2,** 45–60
5. Hirata, Y., Kawachi, T., and Sugimura, T. (1967) *Biochim. Biophys. Acta* **144,** 233–241
6. Trulson, M. E., and Sampson, H. W. (1986) *J. Nutr.* **116,** 1109–1115
7. Fears, R., and Murrell, E. A. (1980) *Br. J. Nutr.* **43,** 349–356
8. Toye, A. A., Dumas, M. E., Blancher, C., Rothwell, A. R., Fearnside, J. F., Wilder, S. P., Bihoreau, M. T., Cloarec, O., Azzouzi, I., Young, S., Barton, R. H., Holmes, E., McCarthy, M. I., Tatoud, R., Nicholson, J. K., Scott, J., and Gauguier, D. (2007) *Diabetologia* **50,** 1867–1879
9. Nocito, A., Dahm, F., Jochum, W., Jang, J. H., Georgiev, P., Bader, M., Renner, E. L., and Clavien, P. A. (2007) *Gastroenterology* **133,** 608–618
10. Lang, P. A., Contaldo, C., Georgiev, P., El-Badry, A. M., Recher, M., Kurrer, M., Cervantes-Barragan, L., Ludewig, B., Calzascia, T., Bolinger, B., Merkler, D., Odermatt, B., Bader, M., Graf, R., Clavien, P. A., Hegazy, A. N., Löhning, M., Harris, N. L., Ohashi, P. S., Hengartner, H., Zinkernagel, R. M., and Lang, K. S. (2008) *Nat. Med.* **14,** 756–761
11. Lesurtel, M., Soll, C., Graf, R., and Clavien, P. A. (2008) *Cell Mol. Life Sci.* **65,** 940–952
12. Yu, P. L., Fujimura, M., Okumiya, K., Kinoshita, M., Hasegawa, H., and Fujimiya, M. (1999) *J. Comp. Neurol.* **411,** 654–665
13. Facer, P., Polak, J. M., Jaffe, B. M., and Pearse, A. G. (1979) *Histochem. J.* **11,** 117–121
14. Kubovcakova, L., Krizanova, O., and Kvetnansky, R. (2004) *Neuroscience* **126,** 375–380
15. Guo, F., and Cavener, D. R. (2007) *Cell Metab.* **5,** 103–114
16. Macotela, Y., Emanuelli, B., Bång, A. M., Espinoza, D. O., Boucher, J., Beebe, K., Gall, W., and Kahn, C. R. (2011) *PLoS One* **6,** e21187
17. Laplante, M., and Sabatini, D. M. (2009) *Curr. Biol.* **19,** R1046–1052
18. Khamzina, L., Veilleux, A., Bergeron, S., and Marette, A. (2005) *Endocrinology* **146,** 1473–1481
19. Li, S., Brown, M. S., and Goldstein, J. L. (2010) *Proc. Natl. Acad. Sci. U.S.A.* **107,** 3441–3446
20. Chang, G. R., Chiu, Y. S., Wu, Y. Y., Chen, W. Y., Liao, J. W., Chao, T. H., and Mao, F. C. (2009) *J. Pharmacol. Sci.* **109,** 496–503
21. Dennis, P. B., Fumagalli, S., and Thomas, G. (1999) *Curr. Opin. Genet. Dev.* **9,** 49–54
22. Raught, B., Gingras, A. C., and Sonenberg, N. (2001) *Proc. Natl. Acad. Sci. U.S.A.* **98,** 7037–7044
23. Finn, P. F., and Dice, J. F. (2006) *Nutrition* **22,** 830–844
24. Czaja, M. J. (2010) *Am. J. Physiol. Cell Physiol.* **298,** C973–C978
25. Singh, R., Kaushik, S., Wang, Y., Xiang, Y., Novak, I., Komatsu, M., Tanaka, K., Cuervo, A. M., and Czaja, M. J. (2009) *Nature* **458,** 1131–1135
26. Osawa, Y., Uchinami, H., Bielawski, J., Schwabe, R. F., Hannun, Y. A., and Brenner, D. A. (2005) *J. Biol. Chem.* **280,** 27879–27887
27. Osawa, Y., Seki, E., Adachi, M., Suetsugu, A., Ito, H., Moriwaki, H., Seishima, M., and Nagaki, M. (2010) *Hepatology* **51,** 237–245
28. Osawa, Y., Seki, E., Kodama, Y., Suetsugu, A., Miura, K., Adachi, M., Ito, H., Shiratori, Y., Banno, Y., Olefsky, J. M., Nagaki, M., Moriwaki, H., Brenner, D. A., and Seishima, M. (2011) *FASEB J.* **25,** 1133–1144
29. Osawa, Y., Hannun, Y. A., Proia, R. L., and Brenner, D. A. (2005) *Hepatology* **42,** 1320–1328
30. Hoshi, M., Saito, K., Hara, A., Taguchi, A., Ohtaki, H., Tanaka, R., Fujigaki, H., Osawa, Y., Takemura, M., Matsunami, H., Ito, H., and Seishima, M. (2010) *J. Immunol.* **185,** 3305–3312
31. Liu, H. Y., Han, J., Cao, S. Y., Hong, T., Zhuo, D., Shi, J., Liu, Z., and Cao, W. (2009) *J. Biol. Chem.* **284,** 31484–31492
32. Matthies, D. L., and Jacobs, F. A. (1993) *J. Nutr.* **123,** 852–859
33. Lim, J. S., Mietus-Snyder, M., Valente, A., Schwarz, J. M., and Lustig, R. H. (2010) *Nat. Rev. Gastroenterol. Hepatol.* **7,** 251–264
34. Forrest, C. M., Mackay, G. M., Stoy, N., Egerton, M., Christofides, J., Stone, T. W., and Darlington, L. G. (2004) *Free Radic. Res.* **38,** 1167–1171
35. Feksa, L. R., Latini, A., Rech, V. C., Wajner, M., Dutra-Filho, C. S., de Souza Wyse, A. T., and Wannmacher, C. M. (2006) *Neurochem. Int.* **49,** 87–93
36. Drakos, E., Rassidakis, G. Z., and Medeiros, L. J. (2008) *Expert Rev. Mol. Med.* **10,** e4
37. Stiles, B., Wang, Y., Stahl, A., Bassilian, S., Lee, W. P., Kim, Y. J., Sherwin, R., Devaskar, S., Lesche, R., Magnuson, M. A., and Wu, H. (2004) *Proc. Natl. Acad. Sci. U.S.A.* **101,** 2082–2087
38. Reiter, A. K., Anthony, T. G., Anthony, J. C., Jefferson, L. S., and Kimball, S. R. (2004) *Int. J. Biochem. Cell Biol.* **36,** 2169–2179
39. Lynch, C. J., Halle, B., Fujii, H., Vary, T. C., Wallin, R., Damuni, Z., and Hutson, S. M. (2003) *Am. J. Physiol. Endocrinol. Metab.* **285,** E854–E863
40. Lynch, C. J., Hutson, S. M., Patson, B. J., Vaval, A., and Vary, T. C. (2002) *Am. J. Physiol. Endocrinol. Metab.* **283,** E824–E835
41. Wilson, F. A., Suryawan, A., Orellana, R. A., Gazzaneo, M. C., Nguyen, H. V., and Davis, T. A. (2011) *Amino Acids* **40,** 157–165
42. Soll, C., Jang, J. H., Riener, M. O., Moritz, W., Wild, P. J., Graf, R., and Clavien, P. A. (2010) *Hepatology* **51,** 1244–1254

The FASEB Journal • Research Communication

Acid sphingomyelinase regulates glucose and lipid metabolism in hepatocytes through AKT activation and AMP-activated protein kinase suppression

Yosuke Osawa,*,†,[1] Ekihiro Seki,§ Yuzo Kodama,§ Atsushi Suetsugu,† Kouichi Miura,§ Masayuki Adachi,§ Hiroyasu Ito,* Yoshimune Shiratori,† Yoshiko Banno,‡ Jerrold M. Olefsky,§ Masahito Nagaki,† Hisataka Moriwaki,† David A. Brenner,§ and Mitsuru Seishima*

*Department of Informative Clinical Medicine, †Department of Gastroenterology, and ‡Department of Cell Signaling, Gifu University Graduate School of Medicine, Gifu, Japan; and §Department of Medicine, University of California–San Diego School of Medicine, La Jolla, California USA

ABSTRACT **Acid sphingomyelinase (ASM) regulates the homeostasis of sphingolipids, including ceramides and sphingosine-1-phosphate (S1P). Because sphingolipids regulate AKT activation, we investigated the role of ASM in hepatic glucose and lipid metabolism. Initially, we overexpressed ASM in the livers of wild-type and diabetic *db/db* mice by adenovirus vector (Ad5ASM). In these mice, glucose tolerance was improved, and glycogen and lipid accumulation in the liver were increased. Using primary cultured hepatocytes, we confirmed that ASM increased glucose uptake, glycogen deposition, and lipid accumulation through activation of AKT and glycogen synthase kinase-3β. In addition, ASM induced up-regulation of glucose transporter 2 accompanied by suppression of AMP-activated protein kinase (AMPK) phosphorylation. Loss of sphingosine kinase-1 (SphK1) diminished ASM-mediated AKT phosphorylation, but exogenous S1P induced AKT activation in hepatocytes. In contrast, SphK1 deficiency did not affect AMPK activation. These results suggest that the SphK/S1P pathway is required for ASM-mediated AKT activation but not for AMPK inactivation. Finally, we found that treatment with high-dose glucose increased glycogen deposition and lipid accumulation in wild-type hepatocytes but not in $ASM^{-/-}$ cells. This result is consistent with glucose intolerance in $ASM^{-/-}$ mice. In conclusion, ASM modulates AKT activation and AMPK inactivation, thus regulating glucose and lipid metabolism in the liver.—Osawa, Y., Seki, E., Kodama, Y., Suetsugu, A., Miura, K., Adachi, M., Ito, H., Shiratori, Y., Banno, Y., Olefsky, J. M., Nagaki, M., Moriwaki, H., Brenner, D. A., Seishima, M. Acid sphingomyelinase regulates glucose and lipid metabolism in hepatocytes through AKT activation and AMP-activated protein kinase suppression. *FASEB J.* 25, 1133–1144 (2011). www.fasebj.org**

Key Words: sphingosine-1-phosphate · glucose intolerance · glucose transporter 2 · glycogen synthase kinase-3β

THE LIVER IS A KEY ORGAN for glucose and lipid metabolism. During feeding, hepatocytes increase glucose uptake in response to elevated glucose levels in the portal vein and increase glycogen and triacylglyceride synthesis. AKT is a key molecule for insulin signaling and glucose metabolism. On AKT activation, glucose influx is stimulated by activation of glycogen synthesis through glycogen synthase kinase (GSK)-3β. The facilitative glucose transporter (GLUT) 2 is predominantly expressed in the liver (1). Hepatic GLUT2 is located at the plasma membrane even in the absence of insulin stimulation; glucose uptake by GLUT2 is therefore not directly affected by insulin. Glucose increases GLUT2 mRNA levels in hepatocytes (2), resulting in increased glucose influx. Constitutive activity of AMP-activated protein kinase (AMPK) decreases glycogen synthesis accompanied by down-regulation of GLUT2 expression (3). Therefore, both AKT and AMPK are involved in glucose metabolism.

Acid sphingomyelinase (ASM) deficiency leads to Niemann-Pick disease. ASM has been reported to be involved in various cellular functions (4), including glucose and lipid metabolism. ASM activity is increased in the serum of type 2 diabetic patients (5). Sphingomyelinase induces GLUT4 translocation to the plasma membrane (6, 7) and increases glucose uptake by adipocytes (7, 8). A high-fat, high-cholesterol diet does not induce hepatic triacylglyceride accumulation in ASM-deficient mice ($ASM^{-/-}$) under an LDL receptor-deficient condition (9). ASM hydrolyzes sphingomyelin to ceramide and phosphorylcholine. Ceramide has been identified as a bioactive mediator in various

[1] Correspondence: Department of Informative Clinical Medicine, Gifu University Graduate School of Medicine, 1-1 Yanagido, Gifu, 501-1194, Japan. E-mail: osawa-gif@umin.ac.jp

doi: 10.1096/fj.10-168351

This article includes supplemental data. Please visit *http://www.fasebj.org* to obtain this information.

cellular functions, including apoptosis and the cell cycle (10, 11). Ceramide accumulation contributes to the development of type 2 diabetes (12). Indeed, inhibition of ceramide synthesis by myriocin, serine palmitoyltransferase inhibitor, or dihydroceramide desaturase improves insulin resistance induced by glucocorticoid or saturated fat (13). Ceramide induces insulin resistance by inactivation of AKT through protein phosphatase-2A and PKC-ζ (14, 15) or by inhibition of AKT translocation to the plasma membrane (16). In addition, ceramide inhibits AMPK activation in hepatoma cells (17).

Not only ceramide but also its metabolite sphingosine-1-phosphate (S1P) is involved in glucose metabolism. Ceramide is hydrolyzed by ceramidase to sphingosine, which is further phosphorylated to S1P by sphingosine kinase (SphK; ref. 18). S1P stimulates AKT activation in human (19) and rodent hepatocytes (20) through the S1P receptor (S1PR). S1P signaling also increases glucose uptake *via* the insulin receptor and production of reactive oxygen species in C2C12 mouse myoblast cells (21). Because sphingolipids are important in glucose and lipid metabolism, we investigated the role of ASM in glucose and lipid metabolism in hepatocytes. In this study, we determined that ASM stimulates glucose uptake, glycogen deposition, and lipid accumulation *via* S1P formation and subsequent AKT activation. As a result, ASM deficiency causes glucose intolerance.

MATERIALS AND METHODS

Animals

The experiments were conducted in accordance with the institutional guidelines of Gifu University and Columbia University. Sprague-Dawley male rats and male wild-type (C57BL/6J), $ASM^{-/-}$, SphK1-deficient ($SphK1^{-/-}$; refs. 20, 22), and obese and diabetic *db/db* mice (C57BL/6 background) were used for this study.

Mice

$ASM^{-/-}$ mice (C57BL/6 background) and $SphK1^{-/-}$ mice (C57BL/6 background) (23), which lack the putative lipid kinase catalytic domain, were bred for studies. Obese and diabetic *db/db* mice (C57BL/6 background) were obtained from the Institute for Animal Reproduction (Ibaragi, Japan), and wild-type C57BL/6J mice were from Japan SLC (Shizuoka, Japan). Eight- to 10-wk-old male mice were used for *in vivo* studies.

Intraperitoneal glucose tolerance test (IPGTT)

The 8- to 10-wk-old male mice (wild-type, *db/db*, or $ASM^{-/-}$ mice) were deprived of food for 18 h. D-Glucose (2 mg/g body weight) was injected intraperitoneally, and blood glucose levels were monitored at 0, 30, 60, and 120 min after the injection using G checker (Sanko Junyaku, Tokyo, Japan). Values for area under the blood glucose curve after glucose loading were calculated. Serum insulin content was measured with a mouse insulin ELISA kit (Shibayagi, Gunma, Japan).

Primary hepatocyte cultures

Sprague-Dawley male rats (200–250 g) or mice (4 wk old) were anesthetized with ketamine and xylazine administered by intraperitoneal injection. Hepatocytes were then isolated by a nonrecirculating *in situ* collagenase perfusion of livers cannulating through the portal vein of rats or inferior vena cava of mice. Livers were first perfused *in situ* with 0.5 mM EGTA containing calcium-free salt solution, followed by perfusion with solution containing 0.02% collagenase D (Roche Diagnostics, Indianapolis, IN, USA). The liver was then gently minced on a Petri dish and filtered with polyamide mesh (3-60/42; Sefar America Inc., New York, NY, USA). Hepatocytes were washed 3 times and centrifuged at 50 *g* for 1 min. Cell viability was consistently >90%, as determined by trypan blue exclusion. Cells were plated on dishes coated with rat collagen type I in Waymouth medium (Invitrogen, Carlsbad, CA, USA) containing 10% fetal bovine serum with antibiotics (plating medium).

Cell treatment

After isolation from rat or mouse livers, hepatocytes were cultured in 10% FBS-containing medium for 4 h. Cells were then washed twice with PBS and changed to serum-free RPMI 1640 (Invitrogen) containing glucose (200 mg/dl) and antibiotics in the presence or absence of recombinant adenoviruses [10 plaque forming units (PFU)/cell]. After a 2-h incubation, the culture medium was changed to serum-free RPMI 1640 containing antibiotics, and the cells were incubated for an additional 16 h. Before stimulation with ASM (1 IU/ml; Sigma-Aldrich, St. Louis, MO, USA), SIP (1 μM; Sigma-Aldrich), or high-dose glucose (600 mg/dl), the cells were washed twice with PBS. The cells were pretreated with imipramine (50 μM; Sigma-Aldrich) for 1 h or with pertussis toxin (PTX) (Sigma-Aldrich) for 16 h in some experiments. The hepatocytes were then treated with or without ASM, SIP, or high-dose glucose, and incubated 8 h for glycogen, RNA, and protein extraction or 24 h for Oil Red O staining and triglyceride measurement. The experimental design is shown in Supplemental Fig. S1*A*.

Recombinant adenoviruses

The adenovirus 5 (Ad5) variants Ad5GFP, Ad5CA-AKT, Ad5DN-AKT, Ad5CA-AMPK, and Ad5DN-AMPK express green fluorescent protein (GFP), constitutively active (CA)-AKT encoding an amino-terminal myristylation signal, dominant-negative (DN)-AKT, c-*myc*-CA-AMPK, and c-*myc*-DN-AMPK, respectively (20, 24). The recombinant replication deficient adenovirus Ad5ASM expressing ASM was constructed by an AdEasy Adenoviral Vector System (Stratagene, La Jolla, CA, USA). In brief, the full length of human ASM DNA was subcloned into pTrack adenoviral vector. The plasmid DNA was prepared by the alkaline lysis method and transfected into BJ5183-AD-1 electroporation-competent cells. The virus was grown in HEK293 cells and purified by banding twice on CsCl gradients, then dialyzed and stored at −20°C. The pTrack plasmid contains a GFP sequence driven under a CMV promoter, and the Ad5ASM expresses both ASM and GFP. Mice were infected with the adenoviruses (5×10^8 PFU/mouse) by intravenous injection. IPGTT was performed on 3 d after the infection. The animals were humanely killed at 3 d for glycogen and protein extraction and at 7 d for Oil Red O staining and triglyceride measurement.

Glucose uptake

Primary cultured hepatocytes were treated with or without ASM for 2 h or infected with Ad5ASM or Ad5GFP, and then

2-deoxy-D-[1-^{3}H]glucose (2 μCi/ml; Amersham Biosciences, Piscataway, NJ, USA) was added to the culture medium. After a further 1-h incubation, cells were washed 3 times with ice-cold PBS and lysed in 1% SDS and 200 mM NaOH. The amount of labeled glucose taken up was determined by scintillation counting.

Measurement of glycogen content

After the treatment of hepatocytes for the indicated periods, the dish was placed on ice, washed with ice-cold PBS twice, and then incubated with 30% KOH for 30 min at room temperature. For the measurement of glycogen content in liver tissue, frozen liver tissues were homogenized in 30% KOH. Then, ethanol was added to the lysate, and glycogen was precipitated by centrifugation. The pellet was dissolved with H_2O, and glycogen content was determined by anthrone reagent (2 mg anthrone/ml sulfuric acid). Glucose solution was used as a standard.

Oil Red O staining

For lipid droplet staining, the cells were fixed with 10% formalin and stained with Oil Red O working solution. Hematoxylin was used for counterstaining. For liver tissue, the frozen liver sections were cut at a thickness of 5 μm on a cryostat and stained with Oil Red O.

Measurement of triglyceride

After the treatment, the primary cultured hepatocytes were washed with PBS and scraped with methanol. For the measurement of triglyceride in liver tissue, frozen liver tissues were homogenized in PBS, and methanol was added to the lysate. The lipids were extracted by the method of Bligh and Dyer (25), and triglyceride content was measured using a triglyceride kit (L-type TG M with lipid calibrator; Wako, Osaka, Japan).

Western blot

For the preparation of total cell proteins, cells or frozen liver tissues were homogenized in radioimmunoprecipitation assay buffer (50 mM Tris-HCl, pH 8.8; 150 mM NaCl; 10 mM EGTA; 1% Triton-X; 0.1% SDS; 1% deoxycholic acid; 0.3 mM PMSF; 1 mM sodium orthovanadate; 10 mM sodium fluoride; 0.1 mM sodium molybdate; and 0.5 mM 4-deoxypyridoxine). The proteins were separated by SDS-PAGE and were electrophoretically transferred onto nitrocellulose membrane. The membranes were first incubated with the primary antibodies, anti-phosphorylated-AKT (Ser-473; 9271; Cell Signaling Technology, Danvers. MA, USA), AKT (9272; Cell Signaling), phosphorylated-GSK3β (Ser-9, 9336; Cell Signaling), GSK3β (610201; BD Biosciences, San Jose, CA, USA), phosphorylated-AMPKα (Thr-172, 2531; Cell Signaling), AMPKα (2603; Cell Signaling), GLUT2 (sc-9116; Santa Cruz Biotechnology, Santa Cruz, CA, USA), ASM (sc-11352; Santa Cruz Biotechnology), and β-actin (Sigma-Aldrich) antibodies. Then, the membrane was incubated with the horseradish peroxidase-coupled secondary antibodies (Santa Cruz Biotechnology). Detection was performed with an ECL system (Amersham Biosciences), and the protein bands were quantified by densitometry using the ImageJ program (U.S. National Institutes of Health; http://rsb.info.nih.gov/ij/).

Quantitative real-time RT-PCR

Extracted RNA from the cells was reverse-transcribed, and quantitative real-time PCR with probe-primer sets of GLUT2 and 18S ribosomal RNA (Applied Biosystems, Foster City, CA, USA) was performed using TaqMan analysis (ABI Prism 7000; Applied Biosystems). The changes were normalized based on 18S.

Mass spectrometric analysis of sphingolipids

Electrospray ionization tandem mass spectrometry analysis was performed on a Thermo Finnegan TSQ 7000 triple quadruple mass spectrometer (Thermo Finnegan, San Jose, CA, USA), operating in multiple reaction monitoring positive ionization mode, as reported previously (26).

S1P formation

Primary rat hepatocytes were incubated with [^{3}H]serine (2 μCi/ml)-containing medium for 12 h. Then, the medium was changed to serum-free RPMI 1640 medium containing [^{3}H]serine with subsequent incubation with adenoviruses for an additional 18 h. The cellular lipids were extracted by the method of Bligh and Dyer (25) and separated on TLC plates in the solvent system of 1-butanol/acetic acid/water (60:20:20, v/v). The radiolabeled S1P spot was scraped off from the plates, and the radioactivity was measured in a liquid scintillation counter.

Statistical analysis

The results shown are representative of ≥3 independent experiments. Data are expressed as means ± SD from ≥4 independent experiments. Data between groups were analyzed by Student's t test. Values of $P < 0.05$ were considered statistically significant.

RESULTS

Exogenous ASM improves glucose metabolism in mice

To explore the role of hepatic ASM on glucose and lipid metabolism, an adenovirus vector expressing human ASM, Ad5ASM, was used in this study. On administration of Ad5ASM into mice, ASM was preferentially expressed in the liver but not in muscle and adipose tissue (Supplemental Fig. S1*B, C*). As a result, ASM activity in the liver was increased (Supplemental Fig. S1*D*). Sufficient expression and activity of ASM in Ad5ASM-infected primary cultured hepatocytes were confirmed. This activity efficiently suppressed the level of sphingomyelins in hepatocytes (Supplemental Fig. S1*E* and **Table 1**). Initially, we investigated the effect of ASM in a glucose tolerance test and demonstrated that blood glucose levels were decreased in both wild-type (**Fig. 1*A***) and diabetic *db/db* mice (Fig. 1*B*) in which ASM was overexpressed by Ad5ASM, indicating that ASM improves glucose tolerance. Then, we used primary cultured hepatocytes to investigate the effect of ASM on glucose uptake. Exogenous administration or adenoviral introduction of ASM increased glucose up-

TABLE 1. *Changes in the sphingolipid profile in Ad5ASM-infected hepatocytes*

Species	Ad5GFP	Ad5ASM
C14-SphM	31.5 ± 0.1	22.2 ± 1.8*
C16-SphM	6626.5 ± 261.3	4376.0 ± 210.8*
C18-SphM	2053.2 ± 65.0	1108.7 ± 53.4*
C18:1-SphM	260.9 ± 5.8	168.7 ± 5.1*
C20-SphM	1062.2 ± 20.0	564.4 ± 84.2*
C20:1-SphM	130.0 ± 2.6	79.3 ± 5.5*
C22-SphM	8397.5 ± 538.7	5223.5 ± 688.8*
C22:1-SphM	1221.8 ± 60.2	696.0 ± 109.1*
C24-SphM	24,630.7 ± 115.6	16,310.1 ± 2479.5*
C24:1-SphM	17,194.4 ± 630.6	10,981.6 ± 1385.0*
C14-Cer	5.8 ± 0.6	7.1 ± 1.5
C16-Cer	181.5 ± 7.5	185.3 ± 4.3
C18-Cer	39.3 ± 5.5	50.4 ± 1.3*
C-18:1-Cer	8.4 ± 0.9	10.1 ± 0.1*
C20-Cer	33.0 ± 5.1	42.8 ± 1.5
C24-Cer	919.8 ± 70.5	1140.7 ± 82.5*
C24:1-Cer	547.0 ± 70.3	598.4 ± 3.8
Sph	140.3 ± 19.0	248.6 ± 14.5*

Primary cultured rat hepatocytes were infected with Ad5GFP or Ad5ASM. Sphingomyelin and the different ceramide species were examined by mass spectrometric analysis. Results are expressed as picomoles lipid per milligram protein; they represent means ± SD from 3 independent experiments. SphM, sphingomyelin; Cer, ceramide; Sph, sphingosine. *$P < 0.05$.

take in hepatocytes (Fig. 1*C*), suggesting that ASM improves glucose tolerance by increased hepatic glucose uptake. Next, we examined the role of ASM in glycogen synthesis. Exogenous ASM expression increased hepatic glycogen content *in vivo* (Fig. 1*D*) and *in vitro* (Fig. 1*E*) using primary cultured hepatocytes. We further examined the role of ASM in lipid metabolism. Exogenous ASM introduction increased hepatic lipid content and serum triglycerides (**Fig. 2*A*, *B***) *in vivo*. We verified that ASM induces accumulation of lipid droplets and triglyceride in primary cultured hepatocytes (Fig. 2*C*). These results indicate that ASM contributes not only to glucose uptake but also to the synthesis of glycogen and triglyceride in the liver.

ASM induces AKT activation

AKT is a key molecule in insulin signaling and glucose metabolism. We hypothesized that AKT is involved in ASM-mediated glucose, glycogen, and lipid metabolism. To prove this, we initially investigated whether AKT affects glucose and lipid metabolism in hepatocytes using adenoviral overexpression of DN- or CA-AKT (Ad5DN-AKT and Ad5CA-AKT, respectively). DN-AKT inhibited insulin-induced phosphorylation of AKT, thereby inhibiting glycogen deposition and lipid accumulation by insulin or high-dose glucose in primary cultured hepatocytes (data not shown). In contrast, a constitutively active form of AKT strongly phosphorylated GSK3β (Supplemental Fig. S2*A*), resulting in increased glycogen deposition and lipid accumulation (Supplemental Fig. S2*B* and data not shown). AKT is therefore crucial for glucose and lipid

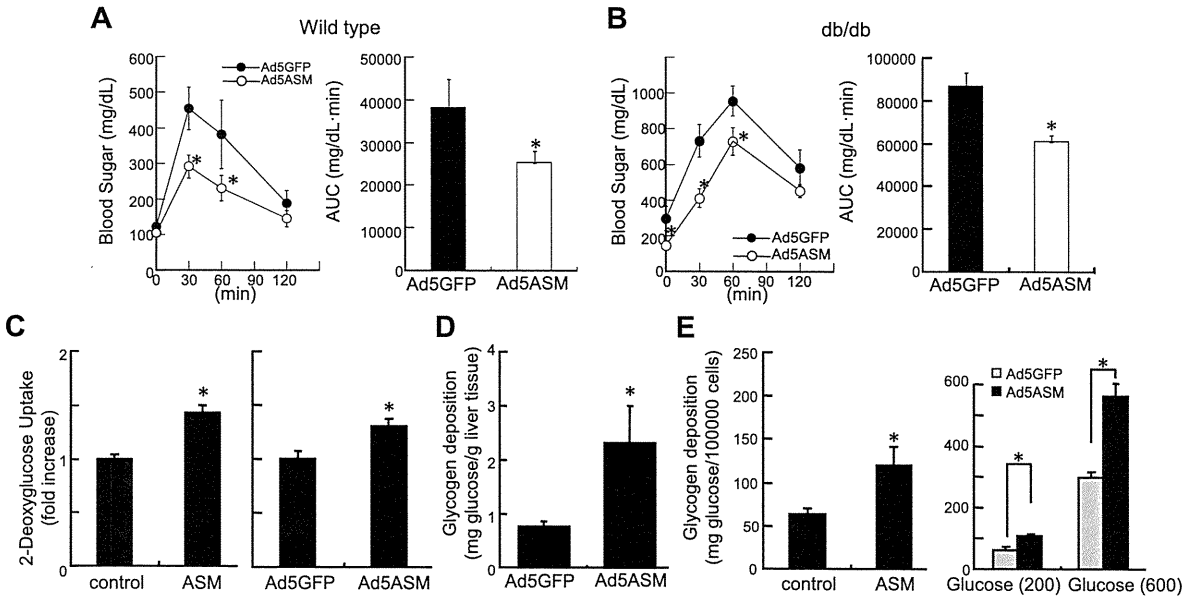

Figure 1. Ad5ASM improves glucose tolerance in mice. *A*, *B*) Wild-type (*A*) or diabetic *db/db* mice (*B*) were infected with Ad5GFP or Ad5ASM (5×10^8 PFU/mouse), then deprived of food for 18 h, and IPGTT was performed by administering a glucose load of 2 mg/g body weight 3 d after the infection. Values of area under the blood glucose curve were calculated (right panels). *C*) Primary cultured rat hepatocytes were treated with ASM (1 U/ml) for 2 h (left panel) or infected with Ad5GFP or Ad5ASM (10 PFU/cell; right panel), followed by measurement of 2-deoxy-D-[1-^{3}H]glucose uptake after a 1-h incubation period. *D*) Hepatic glycogen content in wild-type mice was determined under food-deprivation conditions at 3 d after the adenoviral infection. *E*) Glycogen content was determined in rat hepatocytes at 8 h after ASM treatment (left panel) or normal (200 mg/dl) and high-dose glucose (600 mg/dl) (right panel) treatment with Ad5GFP or Ad5ASM infection. Data are means ± SD from ≥4 independent experiments. *$P < 0.05$.

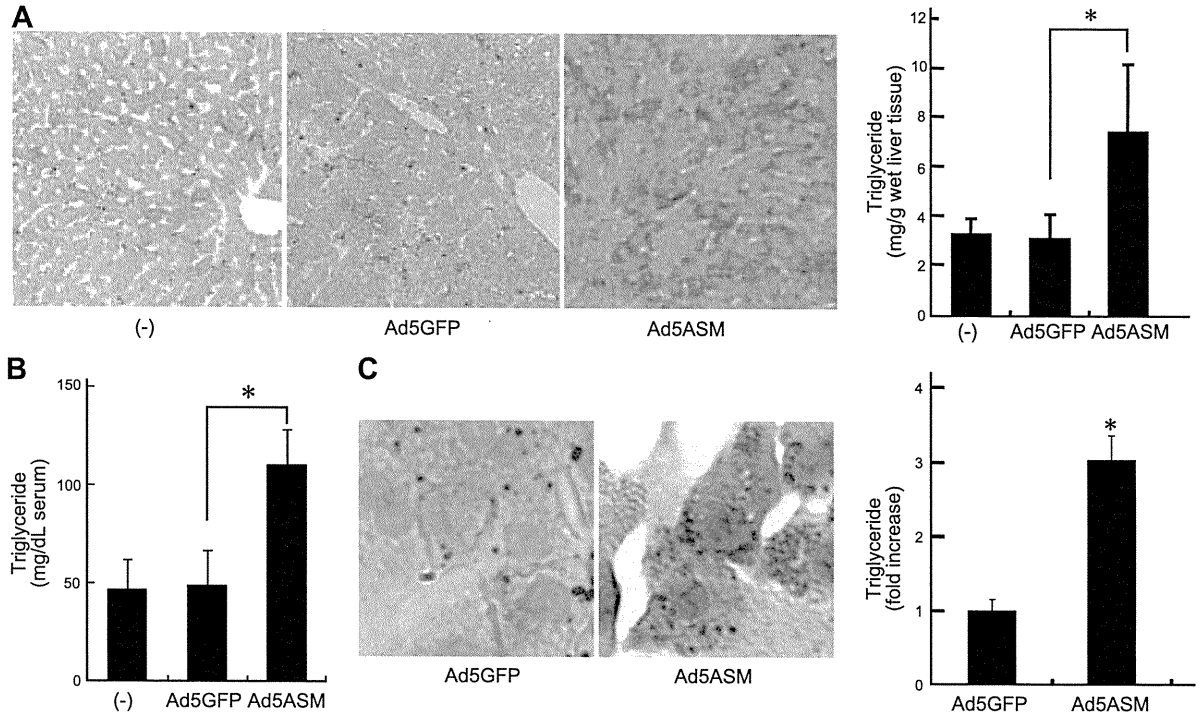

Figure 2. ASM stimulates lipid accumulation. *A*) Wild-type mice were infected with Ad5GFP or Ad5ASM (5×10^8 PFU/mouse). Hepatic lipid content was assessed by Oil Red O staining (left panel; original view ×200) and triglyceride measurement (right panel) in food-deprived wild-type mice at 7 d after the adenovirus infection. *B*) Serum triglycerides were determined in food-deprived wild-type mice at 7 d after the infection. *C*) Primary cultured rat hepatocytes were infected with Ad5GFP or Ad5ASM (10 PFU/cell). Lipid droplets were assessed by Oil Red O staining (original view ×800). Triglyceride level in hepatocytes was determined (right panel). Data are means ± SD from ≥4 independent experiments. $^*P < 0.05$.

metabolism in hepatocytes. On the basis of the fundamental roles of AKT in glucose and lipid metabolism, we investigated the role of AKT in ASM-mediated glucose, glycogen, and lipid metabolism. First, we examined whether ASM alters AKT signaling. Food intake stimulates AKT and GSK3β phosphorylation in mouse liver (**Fig. 3*A***). Introduction of exogenous ASM increased AKT activation under food-deprivation conditions and further increased under feeding conditions (Fig. 3*A*) without increasing serum insulin levels (data not shown) in comparison with control virus-infected animals. We further tested the requirement for insulin in ASM-induced AKT activation. In insulin-free conditions, introduction of ASM still increased AKT and GSK3β phosphorylation in primary cultured rat hepatocytes (Fig. 3*B*, left panel). High-dose glucose did not affect AKT and GSK3β phosphorylation in primary hepatocytes (Fig. 3*B*, left panel). These results suggest that ASM-induced AKT activation is not mediated by insulin or a response to increased intracellular glucose. In contrast, overexpression of DN-AKT abolished ASM-mediated AKT and GSK3β activity (Fig. 3*B*, right panel). DN-AKT overexpression also abolished ASM-induced glycogen deposition and lipid accumulation (Fig. 3*C, D*). These results suggest that ASM regulates glucose, glycogen, and lipid metabolism *via* activation of AKT.

ASM decreases AMPK phosphorylation and increases GLUT2 expression in hepatocytes

Because AMPK is an important component in glucose metabolism, the effects of ASM on AMPK signaling were examined. Glycogen deposition induced by high-dose glucose was increased by DN-AMPK and reduced by CA-AMPK (Supplemental Fig. S2*C, D*) with no observed effects on AKT and GSK3β phosphorylation (data not shown), indicating that AMPK activation reduced glycogen synthesis; this result is consistent with previous studies (3). Then, we assessed the role of AMPK in ASM-mediated effects. In the control virus-infected livers, food intake did not affect AMPK phosphorylation (**Fig. 4*A***), consistent with a previous report (27). In contrast, introduction of ASM reduced AMPK phosphorylation in response to food intake (Fig. 4*A*). ASM also increased food intake-related GLUT2 protein expression in the liver (Fig. 4*A*). A previous study gave indirect evidence that high glycogen content represses AMPK activation in skeletal muscle (28). However, our data demonstrated that AMPK phosphorylation was reduced by ASM in primary cultured hepatocytes under normal glucose conditions (Fig. 4*B*), in which the glycogen content was lower than that in Ad5GFP-infected cells cultured in high-dose glucose medium (Fig. 1*E*). These results suggest that the AMPK inactivation by ASM is not mediated by a response to increased intracellular glycogen. In primary cultured hepatocytes,

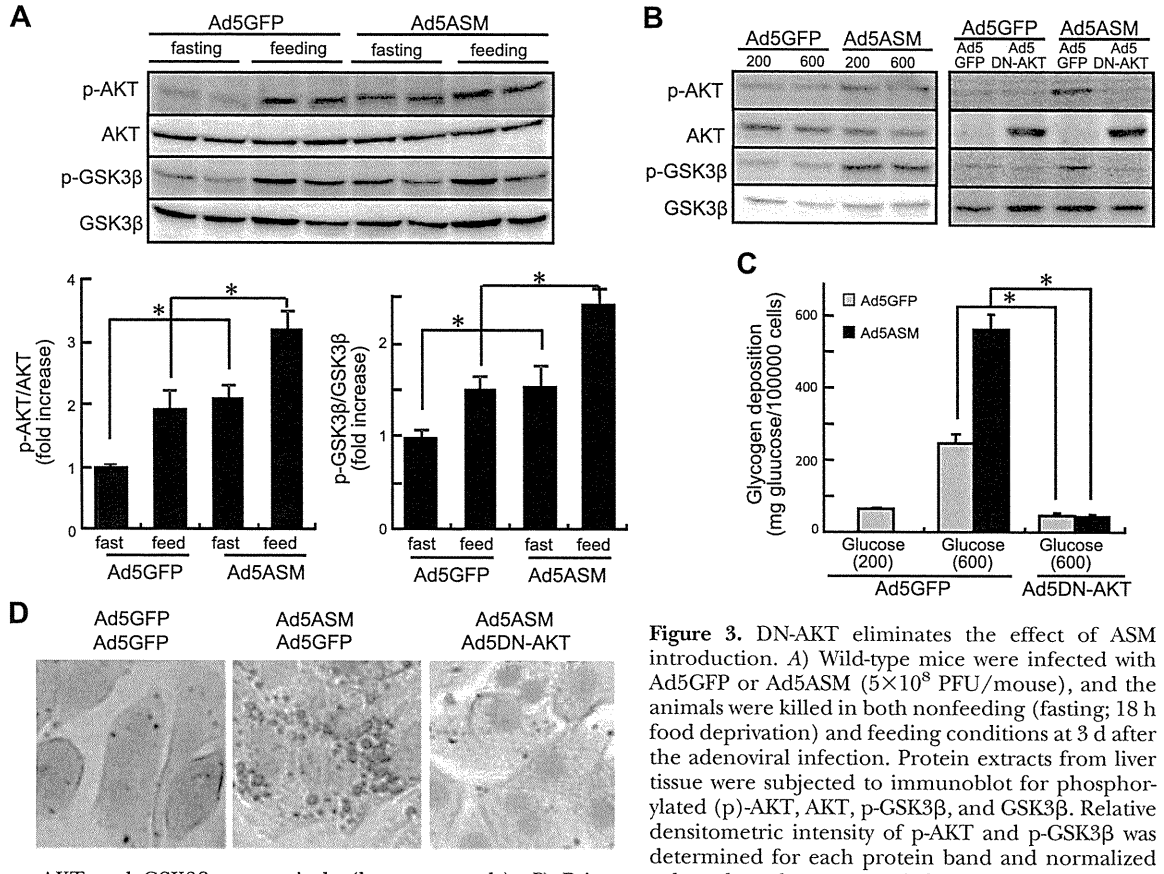

Figure 3. DN-AKT eliminates the effect of ASM introduction. *A*) Wild-type mice were infected with Ad5GFP or Ad5ASM (5×10^8 PFU/mouse), and the animals were killed in both nonfeeding (fasting; 18 h food deprivation) and feeding conditions at 3 d after the adenoviral infection. Protein extracts from liver tissue were subjected to immunoblot for phosphorylated (p)-AKT, AKT, p-GSK3β, and GSK3β. Relative densitometric intensity of p-AKT and p-GSK3β was determined for each protein band and normalized to AKT and GSK3β, respectively (bottom panels). *B*) Primary cultured rat hepatocytes infected with Ad5GFP or Ad5ASM (10 PFU/cell) were further infected with Ad5GFP or Ad5DN-AKT or treated with or without high-dose glucose (600 mg/dl; normal glucose, 200 mg/dl) for 8 h. Protein extracts from hepatocytes were subjected to immunoblot for p-AKT, AKT, p-GSK3β, and GSK3β. *C*) Primary cultured rat hepatocytes infected with Ad5GFP or Ad5ASM plus Ad5GFP or Ad5DN-AKT were treated with or without high-dose glucose. Glycogen content was determined in hepatocytes at 8 h after the high-dose glucose treatment. *D*) Primary cultured rat hepatocytes were infected with Ad5GFP or Ad5ASM plus Ad5GFP or Ad5DN-AKT. Lipid droplets were assessed by Oil Red O staining in hepatocytes (original view ×800). Results shown are representative of ≥3 independent experiments. Data are means ± SD from ≥4 independent experiments. $^*P < 0.05$.

high-dose glucose slightly reduced AMPK phosphorylation (Fig. 4*B*), as shown in a previous report in HepG2 hepatoblastoma cells (29), suggesting that the refractoriness of AMPK by food intake was probably due to systemic mediators. In addition to AMPK, GLUT2 protein and mRNA levels were increased in ASM-expressing primary hepatocytes (Fig. 4*B, C*). CA-AMPK partially inhibited glycogen deposition and lipid accumulation induced by ASM (Fig. 4*D, E*). These results suggest that reduced AMPK activation is also crucial for ASM-mediated glucose metabolism.

ASM activates AKT through the SphK/S1P pathway

ASM hydrolyzes sphingomyelin into ceramide, which is further hydrolyzed and phosphorylated by ceramidase and SphK to form S1P. Because S1P activates AKT in hepatocytes (20), we investigated the contribution of S1P generation to ASM-mediated glucose and lipid metabolism. The ASM-induced phosphorylation of AKT and GSK3β was reduced in SphK1$^{-/-}$ hepatocytes (**Fig. 5*A***). Of note, S1P formation was inhibited in SphK1$^{-/-}$ cells (Fig. 5*B*, left panels). Overexpression of neutral ceramidase (NCD) or exogenous S1P activated AKT (Fig. 5*B*, middle and right panels) in hepatocytes, as we reported previously (20). These results suggest that S1P generated by the breakdown of sphingomyelin contributes to ASM-induced AKT activation. We then examined the involvement of S1PR. Hepatocytes were treated with PTX because S1PRs coupled with G_i are sensitive to PTX. ASM-mediated AKT activation was reduced by PTX treatment (Fig. 5*C*), indicating that ASM generates S1P, which further activates AKT, at least partially *via* S1PRs. ASM-induced glycogen deposition and lipid accumulation were also reduced in SphK1$^{-/-}$ hepatocytes (**Fig. 6*A, B***), whereas the sphingomyelin and ceramide levels were similar to those in wild-type hepatocytes (data not shown). Moreover, SphK1$^{-/-}$ mice did not show hepatic steatosis by exogenous ASM introduction (Fig. 6*C*). In contrast to

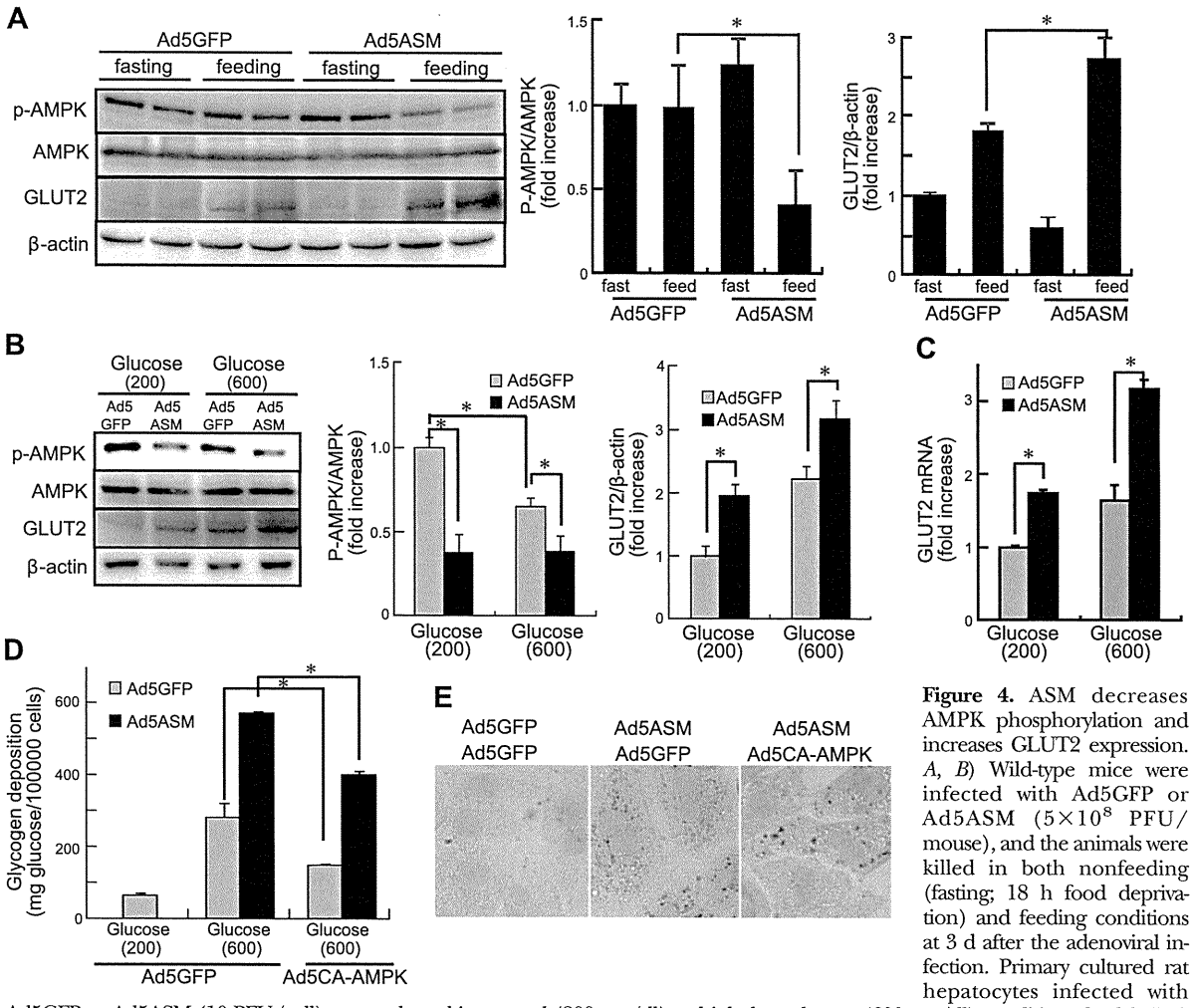

Figure 4. ASM decreases AMPK phosphorylation and increases GLUT2 expression. *A, B*) Wild-type mice were infected with Ad5GFP or Ad5ASM (5×10^8 PFU/mouse), and the animals were killed in both nonfeeding (fasting; 18 h food deprivation) and feeding conditions at 3 d after the adenoviral infection. Primary cultured rat hepatocytes infected with Ad5GFP or Ad5ASM (10 PFU/cell) were cultured in normal (200 mg/dl) or high-dose glucose (600 mg/dl) conditions for 8 h. Left panels: protein extracts from the liver tissue (*A*) or the hepatocytes (*B*) were subjected to immunoblot for phosphorylated (p)-AMPK, AMPK, GLUT2, and β-actin. Right panels: relative densitometric intensity of p-AMPK and GLUT2 was determined for each protein band and normalized to AMPK and β-actin, respectively. *C*). mRNA levels of GLUT2 in hepatocytes were determined by quantitative real-time RT-PCR and normalized by 18S ribosomal RNA. *D*) Primary cultured rat hepatocytes infected with Ad5GFP or Ad5CA-AMPK were further infected with Ad5GFP or Ad5ASM. Cells were then incubated in normal or high-dose glucose conditions for 8 h. Glycogen content in hepatocytes was determined. *E*) Primary cultured rat hepatocytes were infected with Ad5GFP, Ad5CA-AMPK, and/or Ad5ASM. Lipid droplets in hepatocytes were assessed by Oil Red O staining (original view ×800). Results shown are representative of ≥3 independent experiments. Data are means ± SD from ≥4 independent experiments. $^*P < 0.05$.

AKT, AMPK was not affected by S1P administration or NCD overexpression (Fig. 5*B*, middle panel). As in wild-type mice, SphK1$^{-/-}$ mice expressing exogenous ASM showed decreased phosphorylation of AMPK (Fig. 5*A*), indicating that the SphK/S1P pathway is not required for ASM-induced AMPK down-regulation.

ASM deficiency inhibits glucose uptake, glycogen deposition, and lipid accumulation in hepatocytes

Finally, we tested whether ASM deficiency causes glucose intolerance. Sphingomyelin accumulation and ceramide reduction were observed in hepatocytes isolated from ASM$^{-/-}$ mice (Supplemental Table S1). Blood glucose levels in ASM$^{-/-}$ mice were higher than those in ASM$^{+/+}$ mice throughout the IPGTT period without any changes in insulin levels (**Fig. 7**). To further investigate the specific role of ASM in hepatocytes, primary hepatocytes were isolated and treated with high-dose glucose (600 mg/dl), which increased glycogen levels (**Fig. 8*A***). Imipramine, a tricyclic antidepressant, causes proteolysis of the active 72-kDa ASM form, thus inhibiting ASM activity (30). Pretreatment with imipramine inhibited high-dose glucose-induced glycogen deposition (Fig. 8*A*), as did the knockout of ASM in mouse hepatocytes (Fig. 8*B*). Moreover, high-dose glucose increased lipid droplets in primary hepatocytes, and imipramine or ASM deficiency suppressed this effect (Fig. 8*C, D*). These results suggest that high-dose glucose increases glucose uptake, resulting in glycogen deposition and lipid accumulation in hepato-